Journal of Catalysis 437 (2024) 115642

Contents lists available at ScienceDirect

Journal of Catalysis

journal homepage: www.elsevier.com/locate/jcat

Research article

Surface anchoring requirements for vanadia clusters on titanium oxide surfaces and their impact on activity for oxidative dehydrogenation of ethanol

Dongmin Yun [a,c,*], Nicolas R. Jaegers [a,b], Jian Zhi Hu [b], Adrian M. Hucal [c], José E. Herrera [c], Yong Wang [a,b,*]

[a] The Gene and Voiland School of Chemical Engineering and Bioengineering, Washington State University, Pullman, WA 99164, United States
[b] Institute for Integrated Catalysis, Pacific Northwest National Laboratory, Richland, WA 99354, United States
[c] Department of Chemical and Biochemical Engineering, Western University, London, Ontario N6A 5B9, Canada

ARTICLE INFO

Keywords:
Vanadia
in situ Raman
in situ FTIR
Oxidative dehydrogenation of ethanol
Mars-van Krevelen
in situ V-NMR
Titnaium oxynitride
Lattice vacancies

ABSTRACT

Titanium oxide site requirements for the anchoring of catalytically active forms of dispersed vanadia species are investigated. Using a series of oxygen-modified titanium nitride materials, we systematically modify the available vanadia-anchoring moieties on the titanium-bearing support surface. This strategy in turn results in a very narrow size distribution of well-dispersed vanadia clusters anchored on the support. This synthesis technique ensures that only highly dispersed vanadia is present on the catalyst surface even at nominal monolayer coverages. A deeper insight into the catalytic behavior for ethanol partial oxidation of the active vanadia species is obtained by comparing intrinsic kinetic and thermodynamic parameters of kinetically relevant reaction steps (heat of ethanol adsorption, hydrogen abstraction activation energy, and the energetics of catalyst reoxidation). It is found that these parameters are dependent on the relative amount of oxygen in the titanium-bearing support and the resulting distribution of vanadia species, which validates the premise of a potential participation of lattice oxygen atoms of the titania support into the catalytic activity of active vanadia species.

1. Introduction

Recently, investigations of the detailed site requirements of catalytically active supported metal oxides have seen a dramatic rise in prominence, with the aim of understanding the role of the metal-support interface at a fundamental level and to maximize the material's catalytic activity [1–3]. When it comes to revealing active sites (species), metal oxide catalysts are more complex than conventional metal catalysts because of the diverse coordination environment around the metal ion, and their different degree of oligomerization (i.e. monomer, dimer, oligomer, polymer, and bulk), domain size, and varying oxidation states of the metal oxide clusters [4,5]. All these different aspects are partially regulated by catalyst precursor and synthesis technique, though are mainly a strong function of the support selected to anchor the active metal oxide species [6–10]. Reducible metal oxide supports, such as titania (TiO_2) and ceria (CeO_2) are examples of an "active support" that can greatly improve metal oxide catalytic performance in processes involving redox steps such as CO oxidation [11–14], water–gas shift [15], oxidative dehydrogenation of alkanes [16–20], selective reduction of NO_x with NH_3 [21–23], oxidation of SO_2 [24], phthalic anhydride [25] and partial oxidation of alcohols [26–28]. Regardless of the specific type of redox transformation, a large improvement in catalytic activity is observed over a metal or metal oxide if it is anchored on a reducible metal oxide support [16,17,29,30].

The atomic scale identification and quantification of the active species in mixed metal oxide catalyst is, however, challenging. Therefore, molecular-level details of the chemical behavior of the catalytic moieties on reducible metal oxides during turnovers remain hidden. The problem is further complicated when substantial reconstruction take place on the surface of the reducible metal oxides during oxygen atom exchange with the surrounding atmosphere [31]. To address some of these challenges, we have extensively investigated the titania-supported vanadia catalyst (VO_x/TiO_2). Our past work [2,32,33] suggests that not all vanadia sites equally participate in the catalytic redox cycle and that highly dispersed

* Corresponding authors at: The Gene and Voiland School of Chemical Engineering and Bioengineering, Washington State University, Pullman, WA 99164, United States.
E-mail addresses: dongminyun@sk.com (D. Yun), yong.wang@pnnl.gov (Y. Wang).

https://doi.org/10.1016/j.jcat.2024.115642
Received 18 February 2024; Received in revised form 4 July 2024; Accepted 8 July 2024
Available online 9 July 2024

(particularly monomeric and dimeric) vanadia moieties are the most active species for the oxidative dehydrogenation of ethanol at 200 °C. We narrowed our focus to the catalyst reoxidation mechanism and the interaction between the supported vanadia and titania support during the oxidative dehydrogenation of ethanol redox cycle [33], since a balance between *"reducibility"* of the supported vanadia and *"reoxidizability"* of the titania support seems to regulate the vanadia reoxidation step [34]. Our results lead us to propose that the vanadia reoxidation step involves surface lattice oxygen migrating along the titania surface to the reduced vanadia center, which explains the origin of the high activity of the VO_x/TiO_2 system, when compared to vanadia anchored on non-reducible supports. Similar observations by Operando Quick X-ray absorption spectroscopy, recently reported, are in agreement with this hypothesis [35]. All these results drove us to further hypothesize that *only a specific subset of oxygen atoms in titanium oxide actively participate in the redox catalytic cycle.* In this contribution, we take this hypothesis further as we attempt to elucidate the titanium oxide site requirements resulting in the formation of active vanadia species. Based on these observations, a new synthesis strategy is proposed. This strategy directs the control of surface species to highly-dispersed catalytically active vanadia. A deeper insight into the redox activity of active vanadia can thus be gained by generating a catalyst containing only well-dispersed (not highly polymerized) vanadia species, even at coverages near or above monolayer over a reducible metal oxide support. It is well established that the choice of the metal oxide support is critical to controlling the dispersion of vanadia species [4,16]. However, regardless of the choice of metal oxide support, and the possibility of obtaining a narrow distribution of VO_x cluster sizes, the coexistence of vanadia species with varying degree of oligomerization, is usually inevitable [5,16]. In an attempt to overcome these limitations, we aimed to engineer a TiO_2 surface, generated using a mild oxidation treatment of a titanium nitride substrate. This approach leads to the formation of an oxygen-unsaturated titanium oxynitride surface ($TiO_{2x}N_{1-x}$), with a surface that contains oxygen moieties able to selectively anchor vanadia species, hence potentially and indirectly controlling vanadia oligomerization as the surface is not rich in anchoring points for the VO_x clusters. We integrate the synthesis work into a framework whereby intrinsic kinetic parameters of the kinetically relevant steps (reduction and reoxidation) for the oxidative dehydrogenation of ethanol are interrogated and detailed spectroscopic characterization is incorporated.

2. Methods

2.1. Catalyst preparation

2.1.1. Synthesis of TiOxNy supports

A series of TiO_xN_y samples were prepared via dry thermal synthesis. Titanium nitride (TiN, 99.2 %, 20 nm, US Nanomaterials, Inc.) with a specific surface area between 50–80 $m^2 \cdot g^{-1}$ was calcined in an oxidative environment adapting a protocol reported elsewhere [36,37]. In short, about 5.0 g of the TiN nanopowder was loaded on top of a quartz frit, which is supported in the middle of a vertical quartz tube (25.0 mm O. D., 18.0 mm I.D.). The system was treated in dry air (UHP, Praxair, 50 ml•min^{-1}) at different temperatures: 350, 400, 450, 550, and 650 °C for 2 h [37]. These dry oxidation treatments result in the formation of vacancy-rich TiO_2 surface shell, and the bulk likely remains as TiN, in other words a core–shell structure (TiN core and TiO_2 shell from the oxidation of TiN denoted to TiN_xO_y hereafter). The synthesized samples are dark blue, light green, yellow, light yellow and white in color, becoming paler as the oxidation temperature increased, consistent with the incorporation of oxygen in the TiN phase. Further confirmation of a core–shell structure for these materials would require high resolution transmission electron microscopic analysis.

2.1.2. Vo_x supported catalysts

VO_x impregnation over the as-prepared TiN_xO_y supports was carried by incipient wetness impregnation, using aqueous vanadium pentoxide (V_2O_5, Sigma Aldrich, ACS grade) dissolved in 1 M oxalic acid ($C_2H_2O_4$, Sigma Aldrich, ACS grade) containing the desired amount of V (7.2 wt %). After impregnation the samples were dried in an oven at 90 °C overnight, and further calcined at 350 °C for 2 h in flowing air (Praxair, UHP, 50 ml•min^{-1}). The temperature for the calcination was carefully controlled to avoid the incorporation of additional oxygen in the TiN_xO_y support. Additional catalysts with different loadings (0.4, 0.8, 1.5, 3.6, 5.9 wt% as V) were prepared using nano powdered TiO_2 purchased from Sigma-Aldrich (99.7 %, 21 nm primary particle size), The vanadium impregnation protocol followed was the same as for the case of the TiN_xO_y materials, which is described in detail elsewhere [32] (i.e. incipient wetness of a vanadium oxalate precursor, followed up by calcination in dry air, Praxair, UHP, 50 ml•min^{-1}, at 350 °C).

2.2. Catalysts characterization

Multiple techniques were used to characterize both the synthesized TiO_xN_y supports and V/TiO_xN_y materials. To quantify the amount of oxygen atoms, present on the titanium oxynitride support, the mass change experienced by TiN ($TiN + xO_2 \rightarrow TiO_{2x}N_{(1-x)} + x/2N_2$) was monitored by means of thermal gravimetric analysis (TGA). An inert alumina crucible filled with about 5 mg of TiN nanopowder was placed in a thermogravimetric analyzer (Mettler Toledo TGA/SDTA815e). Then temperature was raised from ambient to 900 °C at a ramping rate of 10 °C•min^{-1} in dry air flow (UHP, Praxair, 50 ml•min^{-1}).

Transmission electron microscopic (TEM) measurements were performed in a Thermo Fisher Scientific (TFS) double corrected Spectra Ultra with an Ultra−X EDS detector operated at 300 kV. The scanning transmission electron microscopy (STEM) images and energy dispersive spectroscopy (EDS) maps were acquired using the Velox program from TFS.

Ultraviolet visible (UV–vis) spectroscopy was carried out to monitor the changes in the electronic structure of the supports during the oxidation of the TiN nanopowder. The samples were analyzed in a Cary 4000 UV/Vis instrument from Shimadzu equipped with a Praying Mantis™ diffuse reflectance cell (Harrick Scientific). An in situ reaction chamber was used for these experiments, using spectroscopic grade $BaSO_4$ as a reference. The Tauc plots were derived from the spectroscopic data using an indirect allowed transition formalism, as per the Davis and Mott correlation [38].

In situ diffuse reflectance infrared Fourier transform spectroscopy (DRIFTs) was carried out to characterize the surface functionalities on the surface of titania oxynitride using a FTIR Vertex 70, Bruker, equipped with a MCT detector cooled by liquid N_2 and a diffuse reflectance cell (HVC-DRP-5 in a diffusion reflectance attachment, Harrick Scientific Co.) with an in-situ reaction chamber. The spectra were referenced to a dehydrated KBr (spectroscopic grade, Sigma Aldrich) powder and recorded under controlled temperature continuously with a 4 cm^{-1} resolution and using a total of 256 scans. About 50 mg of undiluted sample was loaded on a stainless-steel screen mesh and heated to 300 °C in flowing of 10 %O_2/He (Praxair, 50 ml •min^{-1}) for 1 h at a rate of 10 °C•min^{-1} then cooled to 25 °C, following this stage the spectrum was recorded. To understand the site requirements for the formation of supported vanadia species, OH functional groups in the TiN_xO_y were exchanged to OD groups using D_2O (Cambridge Isotopes, 99.9 %) at 400 °C. The spectroscopic features in O–H and O-D stretching vibrations were monitored in the 3500–3800 cm^{-1} and 2900–2500 cm^{-1} regions respectively.

In situ Raman spectra were obtained to characterize the structure of the supported vanadia by monitoring vanadyl signals appearing in the 900∼1300 cm^{-1} Raman shift region using a Horiba LabRAM HR Raman microscope equipped with a 532 nm (LP 532, Bentus) laser source and Synapse charge coupled device, and an in situ cell (CCR1000, Linkam). The sample was first dehydrated at 300 °C (linear heating, 10 °C·min^{-1}) under dry air (50 ml•min^{-1}, A-L Compressed Gases Inc, UHP) for 1 hr.

Raman spectra for the dehydrated sample was recorded at 200 °C. Then, liquid ethanol (Sigma Aldrich, 200 proof, 0.1 ml·hr^{-1}) was introduced through an injection port heated at 100 °C. All transfer lines were kept to 100 °C to prevent condensation. X-ray diffraction patterns were collected using a Rigaku SmartLab X-ray powder diffractometer with a Cu-Ka (incident wavelength = 0.15406 nm) radiation source at 40 kV and 20 mA, equipped with in situ cell. The V/TiO_xN_y sample was calcined at 300 °C (ramping rate 10 °C•min^{-1}) in flowing of 10 %O_2/He (Praxair, 50 ml•min^{-1}) for 1 h. Then diffraction patterns were collected at 300 °C from 10 to 80° (2θ) using continuous accumulation with 0.01° step size at a rate of 0.1°•min^{-1}. ^{51}V NMR spectra were collected to characterize the local structure of vanadia species on the catalyst surface. Samples were dehydrated at 300 °C (linear heating, 10 °C·min^{-1}) under 10 % O_2/N_2 (50 ml•min^{-1}) for 1 hr. Post-reaction NMR samples were exposed to ethanol (Sigma Aldrich, 200 proof, 0.1 ml·hr^{-1}) at 200 °C for 1 hr. Oxidized samples were subsequently held at 200 °C in the oxygen stream for 1 hr prior to measurement. The samples were isolated and transferred to an N_2-purged glovebox where they were loaded into the NMR rotors. MAS NMR experiments were conducted with a 600WB Bruker spectrometer employing a commercial 2.5 mm pencil-type MAS probe. ^{51}V NMR spectra were collected with a 3π/16 pulse width of 1.5 μs, a repetition time of 0.2 s, and an acquisition time of 4.096 ms. ^{1}H NMR were collected with a π pulse width of 1.25 μs and a recycle delay of 2 s. 1024 scans were used to confirm the absence of moisture on dehydrated samples. The corresponding Larmor frequencies are 157.778 and 600.143 MHz.

2.3. Catalytic testing for ethanol oxidative dehydrogenation

Before catalytic testing all samples were pressed into wafers, crushed, and sieved to a particle size < 150 μm. Steady-state oxidative dehydrogenation of ethanol experiments was conducted in a continuous flow fixed bed quartz micro reactor (5 mm I.D.) oriented vertically in an electrically heated furnace at atmospheric pressure equipped with a digital PID temperature controller (Digi-Sense). Catalyst samples were supported on quartz wool equipped with K-type thermocouples placed at the vertical center of the catalyst bed on both sides. The catalyst was pretreated using 0.16 °C•sec^{-1} at temperature ramp to reaction temperature and held at this temperature for 30 min under a O_2/He mixture (5 % and 0.5 %O_2, Praxair, UHP, 2.68 cm^3·sec^{-1} before exposing catalysts to the reactants. After this pretreatment step liquid absolute ethanol (Sigma Aldrich, 200 proof) was evaporated into the flowing O_2/He influent stream at 140 °C using a programmable liquid syringe pump (Model, New Era Syringe pump) with the flow adjusted to give the desired ethanol partial pressure (0.5 – 11 kPa). All gas transfer lines before and after the liquid injection port were kept above 140 °C to prevent condensation of reactants and products. Ethanol conversion rates on VO_x/TiO_2 as well as VO_x/TiO_yN_z catalysts were measured at 165 °C, 180 °C, and 195 °C and 200 °C. The flow of the O_2/He mix (either 5 % or 0.5 %) was adjusted by a mass flow controller (Brooks 5850E) during these experiments. The rates of oxidative dehydrogenation of ethanol are reported as total V-atom turnover rates (moles of ethanol converted per total V atom ($*_T$) per second). Chemical species in the feed and reactor effluent stream were measured using an online gas chromatograph (Agilent Micro GC 460) with a micro capillary column (CP5) connected to a micro thermal conductivity detector. Catalytic testing was precisely controlled to keep ethanol conversion at values lower than 20 % along with a wide range of ethanol partial pressures to ensure differential reactor conditions and avoid mass transfer limitations (Weisz-Prater Criterion, Supporting information Section I). The carbon balance was higher than 99.5 %.

3. Results and discussion

3.1. Catalysts characterization

A list of all catalysts tested in this study is presented in Table S1 and Table S2. Titanium nitride (TiN) is thermodynamically stable at ambient temperature, but a surface oxide layer with abundant oxygen vacancies is formed upon its exposure to oxygen at temperatures exceeding 300 °C [37,39]. In fact, in the semiconductor field, the synthesis of titanium oxynitrides via controlled oxidation of TiN has been identified as a preferred method to the nitridation of TiO_2, given the more favorable energetics of molecular oxygen dissolution on TiN compared to azide radicals on TiO_2 [40,41]. The charge difference introduced by the N^{-3} substitution for O^{-2} also brings additional challenges together with the potential generation of anionic vacancy defects due to the use of the strongly reducing azide species [42].

During TiN oxidation, the insertion of O into TiN leads to evolution of gaseous N_2 [43] and formation of a $TiO_{2x}N_{1-x}$ type structure with different degrees of surface oxygen functionalities, which in turn could potentially serve as anchoring points for supported vanadia, controlling its dispersion and structure. From a strictly stoichiometric point of view, complete transformation of pristine TiN to TiO_2 will result in a mass increase of ~29 %. To determine the stoichiometry of the $TiO_{2x}N_{1-x}$ materials synthesized at different temperatures, we monitored the thermogravimetic (TGA) profile of the TiN nanopowder in the presence of oxygen. This strategy enables the calculation of the degree of oxygen exchange in the TiN support (the x value in $TiN + xO_2 \rightarrow TiO_{2x}N_{1-x} + 0.5xN_2$). Figure S1 shows the TGA profile corresponding to the weight gain of TiN from room temperature to 650 °C in 10 %O_2/He flow. The weight gradually increases from 450 °C to 550 °C and reaches a plateau at 23 % weight gain after this temperature. The difference in the weight gain between a theoretical value (29 %) and experimental one (23 %) is likely the result of oxygen diffusion limitations [44,45]. Table S1 summarizes the calculated chemical formula of $TiO_{2x}N_{1-x}$ for the prepared supporting materials, assuming the oxygen exchange in the materials is solely a function of the treatment temperature. From now on, the different contents of oxygen in the modified TiN supports will be referred as "degree of oxidation".

The morphology of these modified TIN supports was evaluated using electron microscopy. Fig. 1 shows a typical TEM micrograph obtained on the TiN sample treated in air at 400 °C, together with high-angle annular dark-field imaging (HAADF) and Ti, N and O EDX mappings. The data suggests the presence of an oxygen rich core shell structure on the materials. The XRD patterns for a series of the oxidized TiN were obtained, as shown in Figure S2. In all $TiO_{2x}N_{1-x}$ materials prepared the TiN diffraction peaks are absent; instead, two strong diffraction peaks were observed at 25.4°, and 47.9° indicating the presence of crystalline anatase (JCPDS 21–1272). For the $TiO_{2x}N_{1-x}$ materials prepared at temperatures above 500 °C, clear diffraction peaks associated with rutile are also observed (JCPDS 21–1276). These results indicate that the oxidation of the TiN nanopowder results in its transformation from TiN to TiO_2. An analogous trend was also observed in a previous study [46] for TiN powders heated in air, in this case the authors proposed that one nitrogen atom is substituted by two oxygen atoms, with the concomitant formation of a vacant cation site. We calculated the average crystalline sizes of the anatase phase using Scherrer's equation on the main diffraction peak at 25.4° (1 0 1), the values obtained are as listed in Table S1. The calculated crystalline sizes for the anatase phase in $TiO_{0.04}N_{0.98}$, $TiO_{0.12}N_{0.94}$, $TiO_{0.80}N_{0.60}$, and $TiO_{1.30}N_{0.35}$, are 9.5, 12.8, 19.0 and 22 nm, respectively. It is worth noting that among all samples, $TiO_{1.30}N_{0.35}$ is geometrically closest in structure to commercial P25 titania nano powder, in terms of crystallite size and the presence of both rutile and anatase phases [39]. Moreover, this analysis indicates thermal treatment of the TiN in air does not result in significant sintering of the TiN nanoparticles. This observation was confirmed in the TEM micrographs obtained for the as received TiN, $TiO_{0.12}N_{0.94}$ and $TiO_{1.3}N_{0.35}$

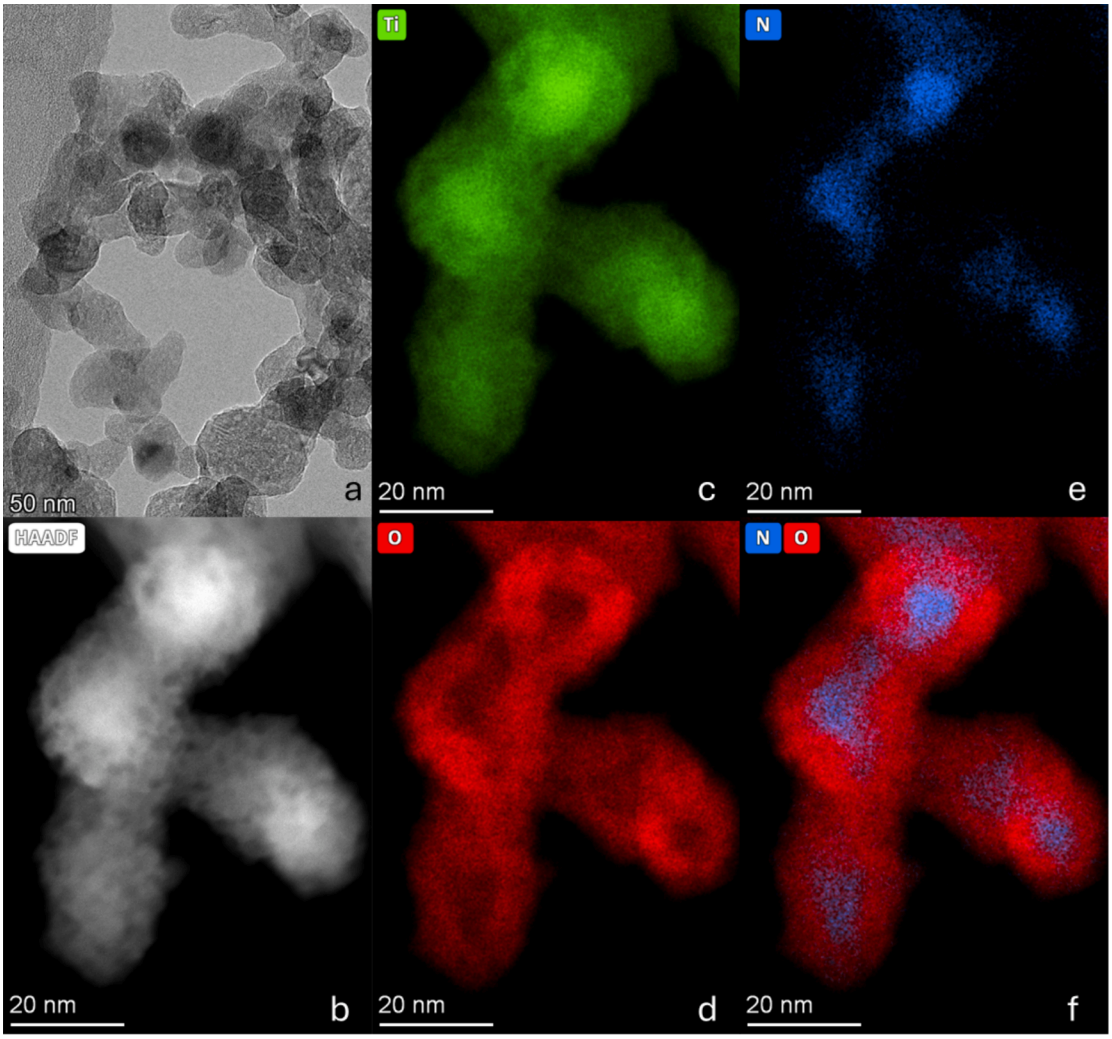

Fig. 1. Typical (a) TEM, (b) HAADF-STEM, and (c-e) EDS elemental mapping images obtained on the $TiO_{0.12}N_{0.94}$ sample (TiN treated in air at 400 °C). The overlay of the N K edge and O K edge signals (f) suggests a core shell structure for the support.

samples (data not shown) where the only difference observed was in terms of the crystalline structure of the sample (treatment at higher temperatures resulted in more defined domains of TiO_2 in the sample, but not in particles of larger size. This specific observation was mirrored in the optical absorption spectra (Fig.S3) obtained on the sample samples, where a clear shift is observed in the absorption maxima (Fig.S3b) associated to TiO_2, resulting from the formation of more ordered TiO_2 domains for samples treated in air at higher temperatures.

3.2. Site requirements for the formation of dispersed and polymeric vanadia: Role of terminal and bridged oxygens in the support

It has been well–documented for supported vanadia/titania systems that the grafting of vanadia moieties on the titania surface occurs by condensing vanadium-bearing precursors at the expense of surface hydroxyl groups present on the titania substrate [47,48]. However, due to the complexity of the surface of titanium oxide in powder form (differently coordinated surface hydroxyls, various facets orientations, etc.) a profound uncertainty in the grafting dynamics remains with respect to how the surface hydroxyl (OH) functional groups present on titania are consumed upon incorporation of vanadia. To provide insight on this and avoid inherent complexities arising from the titania surface heterogeneity, such as accessibility of OH functional groups, we identified the anchoring location of the vanadia species after grafting. We achieved this by monitoring the depletion of surface exchangeable OH functional groups (H/D) of the titania support while increasing vanadia coverage using DRIFTs. For this purpose, the surface OH functional groups of pristine titania and three vanadia/titania samples with different vanadia loadings were isotopically exchanged using deuterated water (D_2O) into OD functional groups at 400 °C (Fig. 2 and Fig.S4 for the remaining deconvoluted bands).

After being exchanged at 400 °C, the IR spectra measured at ambient temperature for OD functional groups present on the pristine TiO_2 (Fig. 2a) shows four deconvoluted peaks at 2739, 2707, 2680, and 2655 cm^{-1}. According to previous literature [49,50], the peak at 2739 cm^{-1} (equivalent to 3715 cm^{-1} as OH functional groups) is assigned to a terminal OD^- bonded to a Ti^{+4} site while the two peaks at 2707 and 2680 cm^{-1} (equivalent to 3660 and 3600 cm^{-1} for OH, respectively) are assigned to bridged OD, which resulted from the protonation of doubly-coordinated O^{-2} sites. The different positions of the linear and bridged hydroxyls reflect the strength of the oxygen-hydrogen (deuterium) bond. As the vanadia was grafted on the support at different coverages, the IR signals corresponding to these relatively acidic OD were still clearly observed (Fig. 2b–d). At 0.4 wt% vanadia loading (Fig. 2b), where highly dispersed vanadia is dominantly present (confirmed by the presence of a single Raman band for vanadyl stretching in dispersed vanadia, Fig.S5), a relatively larger number of terminal linear hydroxyls (2739 cm^{-1} as OD) and a portion of the bridged hydroxyl (2707 cm^{-1}) were consumed. At a higher (1.6 wt%) vanadia loading (Fig. 2c) dispersed and mostly oligomeric vanadia species co-exist, here most of

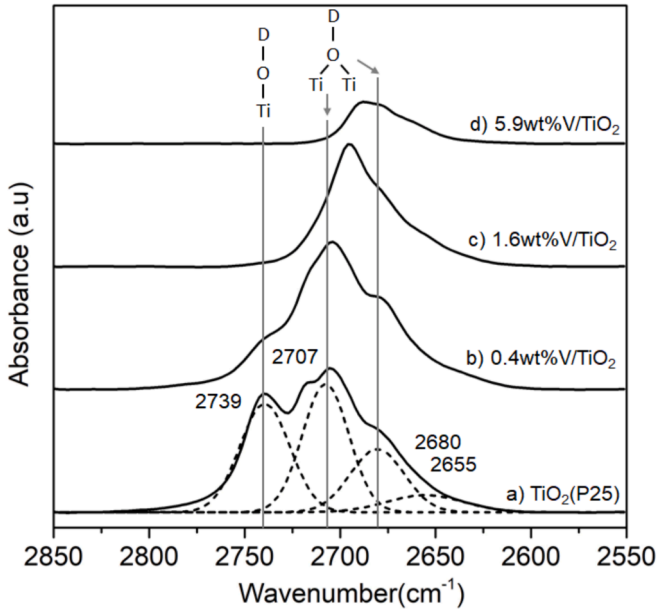

Fig. 2. In situ FTIR spectra of the deuterated hydroxyl groups (OD) vibrations (D_2O exchange at 400 °C, 0.124 kPa, for 1 h for (a) pristine TiO_2 (P25), (b) 0.4 wt%V/TiO_2, (c) 1.6 wt%V/TiO_2 and (d) 5.9 wt%V/TiO_2.

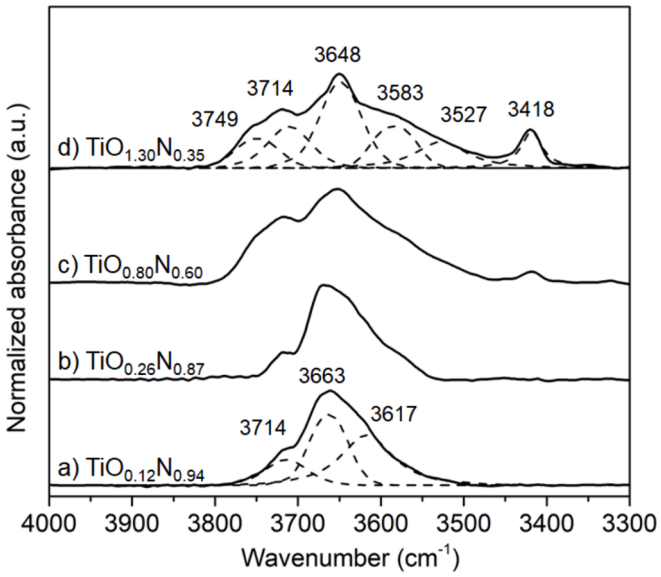

Fig. 3. In situ FTIR spectra of the OH vibrations of (a) $TiO_{0.12}N_{0.94}$, (b) $TiO_{0.26}N_{0.87}$, (c) $TiO_{0.80}N_{0.60}$, (d) $TiO_{1.30}N_{0.35}$, measured at 30 °C after dehydration at 300 °C for 1 h in dry air.

the terminal hydroxyls were eliminated and a significant portion of bridged hydroxyl (2070 cm^{-1}) also disappeared. Lastly, at the highest vanadia loading used (5.9 wt% V, Fig. 2d) most of bridged hydroxyls (2707 and 2680 cm^{-1} as OD) in titania are consumed. These results clearly indicate that the formation of dispersed vanadia on the titania surface does require the use of the terminal linear hydroxyl (2739 cm^{-1}) groups (strongly bonded O–H), and a relatively lower amount of bridged hydroxyl groups (2707 cm^{-1}), while the bridged hydroxyl (weakly bonded O–H) at lower wavenumbers (2680 cm^{-1}) are associated to the formation of polymeric vanadia species and bulk V_2O_5 nano-crystallites. The presence of the peak at 2655 cm^{-1} even at the higher vanadia loadings suggests either the existence of hydroxyl groups accessible to H_2O or D_2O (2.75 Å) but not by vanadia oxalate (7.2 Å), and hence unable to serve as anchoring points for vanadia, or the generation of Brønsted acidic hydroxyl groups.

3.3. *Role of lattice oxygen: Characterization of $TiO_{2x}N_{1-x}$ supports and V/$TiO_{2x}N_{1-x}$ catalysts*

A series of synthesized $TiO_{2x}N_{1-x}$ supports with different degrees of oxidation were characterized using in situ IR experiments to verify the dynamic modification of the OH functional groups incorporated into the TiN material, as these play a critical role in the dispersion of the vanadia surface moieties. These results are presented in Fig. 3 (See Fig. S6 for the remaining deconvoluted bands). Since the total reflectance of each support varies due to the sample color, the IR spectra are presented normalized to the peak of highest intensity on each spectrum. For the $TiO_{0.12}N_{0.94}$ sample (obtained at 400 °C), only three main IR absorption bands were observed at 3714, 3663, and 3617 cm^{-1}. Based on prior assignments, the OH vibrational bands at frequencies higher than 3680 cm^{-1} (3714 cm^{-1} in Fig. 3a) are attributed to terminal linear OH functional groups (equivalent to 2739 cm^{-1} as OD functional groups), while bands at lower frequencies (3663 and 3617 cm^{-1} which are equivalent to 2707, and 2680 cm^{-1}, respectively) are assigned to bridged OH, originated from coordinately unsaturated Ti^{4+} and O^{2-} pairs [50]. The narrow distribution of IR bands assigned to OH functional groups become broader for the support prepared at 500 °C ($TiO_{0.80}N_{0.60}$) and widens further up to 600 °C ($TiO_{1.30}N_{0.35}$); spectral deconvolution suggests vibrations at 3749, 3714, 3648, 3583, 3527, and 3418 cm^{-1}. These additional OH bands observed suggest that at least two different types of linear OH species and four types of bridged OH sites are present in all samples treated at temperatures of 500 °C and above ($TiO_{0.80}N_{0.60}$, $TiO_{1.28}N_{0.36}$, and $TiO_{1.30}N_{0.35}$), which are likely associated to the formation of rutile at higher temperatures, as observed using XRD (Fig. S2).

The supported vanadia catalysts with constant vanadia loading (7.2 wt%; denoted as V/TiO_xN_y afterward) deposited over different TiO_xN_y materials were characterized using multiple spectroscopy techniques. Raman (Fig. 4 left panel) and IR spectra (Fig. 4 right panel) of the dehydrated vanadia species present on the V/$TiO_{2x}N_{1-x}$ catalysts were obtained at 200 °C in situ after pretreating the sample at 350 °C in flowing of dry air. Despite a large number of studies dedicated to interpretation of Raman and IR spectra of supported vanadia moieties, the assignment of precise wavenumbers of Raman and IR vibrational bands to geometrically well-defined cluster structure on powdered samples remains elusive. Nevertheless, spectroscopic assignments of the Raman and IR spectra of vanadyl stretching were attempted using information previously reported in studies of well-defined model structures[32,51]. For the Raman spectra of vanadia on pristine TiO_2, in particular, the vanadyl stretching band of dispersed vanadia species shifts from ~ 1025 cm^{-1} at low vanadia coverage to ~ 1030 cm^{-1} as vanadium coverages increase due to vibrational coupling of vanadyl bonds in close proximity [52]. Based on a careful examination of the reports in the literature, the common Raman bands centered at 1031 cm^{-1} (Fig. 4 left panel) for all V/TiO_xN_y samples indicate the presence of well dispersed vanadia species even at high V coverage. As our data indicates, what is particularly interesting is the sole presence of dispersed vanadia species (samples V/$TiO_{0.04}N_{0.98}$, and V/$TiO_{0.12}N_{0.94}$) fitted with two peaks at 1018 and 1031 cm^{-1} for the cases where vanadia is supported on the titania oxynitride formed at temperatures lower than 450 °C, even at these relatively high (7.2 wt%) vanadia coverage. This result is remarkable, since it is well established that polymerized V_2O_5 nanocrystals form on P25 titania at values above nominal monolayer vanadia coverage (>5.6 wt% VO_x) when a solution of vanadium oxalate precursor is used [53,54].

On the other hand, the Raman spectra obtained for V/$TiO_{0.26}N_{0.87}$, V/$TiO_{0.80}N_{0.60}$ and V/$TiO_{1.30}N_{0.35}$, (Fig. 4c, d and e, left panel), prepared using supports calcined at higher temperatures (450, 500, and 600 °C respectively), show the additional presence of a Raman band at

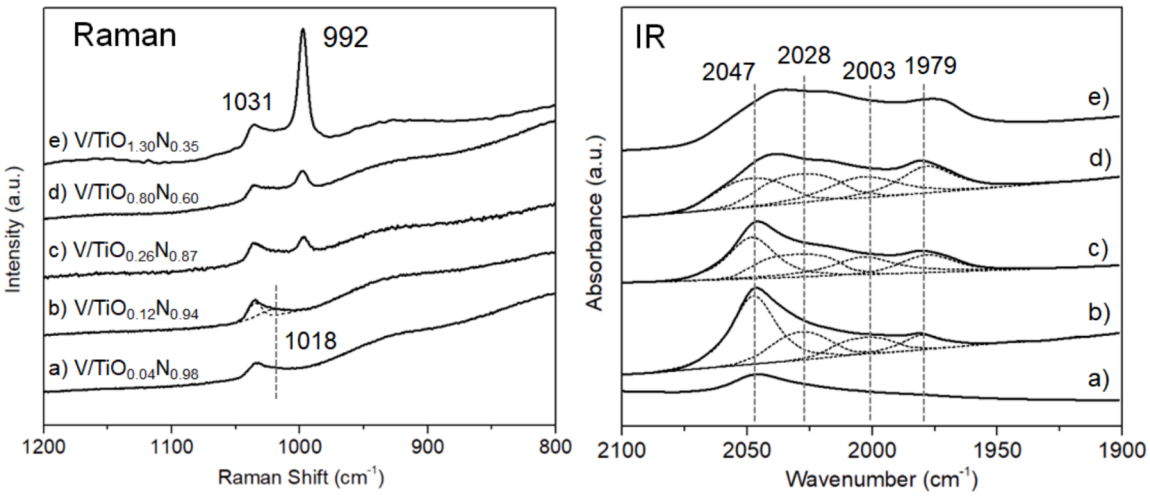

Fig. 4. In situ Raman spectra (left) and DRIFTs (right) of a series of dehydrated (a) $V/TiO_{0.04}N_{0.98}$, (b) $V/TiO_{0.12}N_{0.94}$, (c) $V/TiO_{0.26}N_{0.87}$ (d) $V/TiO_{0.80}N_{0.60}$, and (e) $V/TiO_{1.30}N_{0.35}$ measured at 200 °C after dehydration at 350 °C for 1 h in dry air.

992 cm^{-1}, which is attributed to crystalline V_2O_5 nanoparticles. As indicated above, this band was not observed in the two $V/TiO_{0.04}N_{0.98}$, and $V/TiO_{0.12}N_{0.94}$ samples, which were obtained using supports calcined at lower temperatures (350 °C, Fig. 4a and 400 °C, Fig. 4b). This typical heterogeneous coexistence of VOx clusters (dispersed, oligomeric, polymerized, and nanocrystalline vanadia) with different size is ordinarily observed at high vanadia coverages on pristine TiO_2 supports [20,53,54]. Indeed, in agreement with these and previously reported observations [9,16], the absence of the band at 992 cm^{-1} strongly suggests that isolated VO_x species, are predominantly present on the $V/TiO_{0.04}N_{0.98}$, and $V/TiO_{0.12}N_{0.94}$ samples, as opposed to the case of the samples obtained over the supports calcined at higher temperatures (Fig. 4 left, c, d and e) which contain nanocrystalline VOx species, likely due to polymerization of the vanadium clusters.

The infrared spectra obtained on these samples also provides information on the type of surface vanadia species, through the signal of the V = O first overtone (1900–2100 cm^{-1}). The right panel in Fig. 4 shows the results obtained; a signal centered at 2047 cm^{-1} is dominantly observed for the $V/TiO_{0.04}N_{0.98}$, and $V/TiO_{0.12}N_{0.94}$ (Fig. 4a, and 4b right panel), while a signal with two maximums at 2028 and 1979 cm^{-1} is observed for the case of the $V/TiO_{0.26}N_{0.87}$, $V/TiO_{0.80}N_{0.60}$ and $V/TiO_{1.30}N_{0.35}$ samples (Fig. 4c–4e right panel, respectively). The band at 2047 cm^{-1} has being recently linked to the overtone frequency to monooxo terminations on vanadia clusters anchored on titania [55]. while all other signals have been previously observed [52]. As discussed elsewhere [56], these IR bands can be assigned to vanadia moieties in different states of aggregation, i.e. higher wavenumbers are assigned to the overtone signal of well dispersed vanadia species. A careful inspection of the spectra was made by deconvoluting the obtained IR bands for samples $V/TiO_{0.04}V_{0.98}$ and $V/TiO_{0.12}N_{0.94}$ (Fig. 4 right panel, spectra a) and b) respectively), which as per their Raman bands displayed distinct levels of vanadia dispersion. For this analysis, the peak positions of the deconvoluted IR bands were fixed. Data indicates that the first overtone signal splits into main four bands centered at 2047, 2028, 2003, and 1979 cm^{-1}. The relative intensity of the peak at 2047 cm^{-1}, which is proposed to correspond to monomeric vanadia, reaches a maximum for the case of the $V/TiO_{0.12}N_{0.94}$ sample. On the other hand, the peak at 1979 cm^{-1}, assigned to polymeric vanadia, increases gradually as the oxygen content in the support increases. These trends are unambiguously consistent with the Raman spectra (Fig. 4 left panel). Based on the Raman data we could hypothesize that each of the four IR peaks can be assigned to monomeric, dimeric, oligomeric and polymeric vanadia, respectively.

^{51}V solid state magic angle spinning (MAS) nuclear magnetic resonance (NMR) offers an alternative method to probe supported vanadia catalysts to elucidate the structural environment around the active sites. Advances in magnetic field strength, sample spinning rate, and spectral interpretation have enabled a detailed distinction between unique surface vanadia sites on catalyst supports [20,57,58]. By applying this magnetic resonance technique to these materials, the trends in speciation can be monitored with in situ ^{51}V MAS NMR (Fig. 5, left) by noting differences in chemical shifts and signal intensities among samples and sample treatments. The dehydrated samples prepared on $TiO_{2x}N_{1-x}$ supports calcined at low temperatures ($V/TiO_{0.04}N_{0.98}$, and $V/TiO_{0.12}N_{0.94}$) demonstrate the typical features of well-dispersed vanadia species. Both show signals indicative of monomeric structures at approximately −515 and −530 ppm (tetradehdral and square pyramidal type) [57,59]. Additionally, dimeric and oligomeric species are observed between −560 and −700 ppm, with the $V/TiO_{0.12}N_{0.94}$ sample suggesting a larger amount of the more oligomerized vanadia domains. As the support oxidation temperature was increased to 450 °C or above ($V/TiO_{0.26}N_{0.87}$, $V/TiO_{0.80}N_{0.60}$, and $V/TiO_{1.30}N_{0.35}$), the spectra are dominated by a single well defined narrow peak around −614 ppm which comprises between 63 and 83 % of the observed vanadia signals. Comparing the sideband pattern of these supported samples to that of bulk V_2O_5 (Figure S7) suggests the local chemical environment around these vanadium nuclei is well-aligned with that of the bulk oxide and indicates the formation of highly oligomerized vanadia which may be present at the genesis of nanocrystalline V_2O_5, so we ascribe the −614 ppm signal to bulk V_2O_5 nanoparticles. Evidence of less oligomerized features is still present, including a small quantity (~2%) of monomeric vanadia on $V/TiO_{0.26}N_{0.87}$.

Table S5 (supporting information) summarizes these characterization results. Combining all these results, a clear and detailed picture of the structure of the different V/TiO_xN_y catalysts begins to emerge. The IR spectra for the exchanged OD/OH functional groups of a series of vanadia/titania (Pristine N-free TiO_2) samples prepared at various vanadia loadings revealed that terminal and bridged hydroxyls appearing at high wavenumbers (3715, 3660 and 3600 cm^{-1}) are responsible for anchoring dispersed vanadia, with a preference by well-dispersed vanadia species to anchor on the isolated terminal hydroxyl groups. At the same time the distribution of types of OH functional groups in the different TiO_xN_y supports, synthesized by TiN oxidation, is not identical as that on pristine TiO_2. The terminal hydroxyls are more predominant than bridged hydroxyls at low oxygen content in the TiO_xN_y support, which is beneficial for the presence of dispersed vanadia. As the oxygen content increases in the supports, the bridging hydroxyls, responsible for the formation of polymeric vanadia, continue to

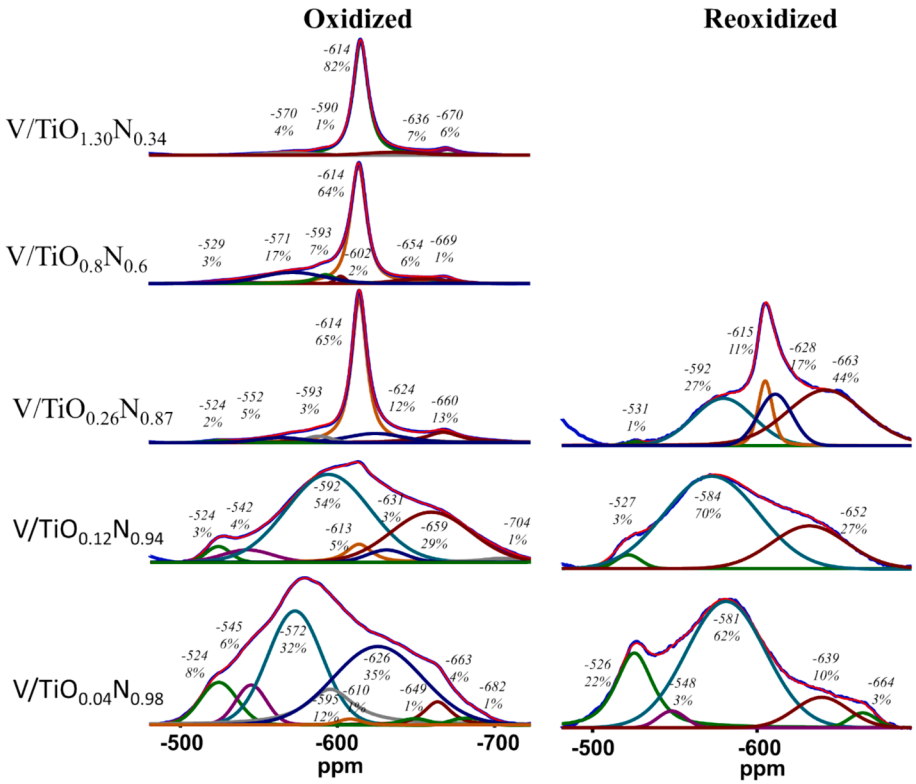

Fig. 5. In situ NMR center band spectra of dehydrated $V/TiO_{0.04}N_{0.98}$, $V/TiO_{0.12}N_{0.94}$, $V/TiO_{0.26}N_{0.87}$, $V/TiO_{0.80}N_{0.60}$, and $V/TiO_{1.30}N_{0.35}$ measured after dehydration at 300 °C for 1 h in dry air (left) and that of select samples after a sequential reduction in dilute ethanol (1.5 kPa, 50 ml•min −1) at 200o C followed by reoxidation in dry air (50 ml•min^{-1}) at 200 °C for one hour (right). Peak positions and centerband species abundance are listed. Dark blue represents experimental data and the red overlay represents the sum of the fit. Green fits around −525 ppm are monomeric. Orange fits around −614 ppm are V_2O_5. Dimers and oligomeric VO_x are present around −540 to −590 ppm and upfield of V_2O_5. (For interpretation of the references to color in this figure legend, the reader is referred to the web version of this article.)

populate. The Raman, IR, and NMR data obtained on a series of V/TiO_xN_y samples with different oxygen/nitrogen content suggests that mostly monomeric vanadia species are present on the two samples with lower oxygen content ($V/TiO_{0.04}N_{0.98}$, $V/TiO_{0.12}N_{0.94}$) obtained on the TiO_xN_y supports prepared by calcining TiN at temperatures below 450 °C. In contrast, both dispersed and polymerized V_2O_5 nanoparticles coexist on the samples obtained using TiN calcined above 450 °C ($V/TiO_{0.80}N_{0.60}$, $V/TiO_{1.28}N_{0.36}$, and $V/TiO_{1.30}N_{0.35}$), all with same V loadings. These observations can be combined to propose a scenario whereby well dispersed vanadia progressively anchors to the lattice-bound oxygen present on the surface support, first at the expense of isolated terminal hydroxyl groups. In other words, a model structure of dispersed vanadia moieties contains oxygen atoms from O-Ti originally present in terminal linear hydroxyl groups (HO-Ti), and from bridged (Ti-O(H)-Ti) titania hydroxyls.

3.4. Assessing activity rates for CH_3CH_2OH oxidative dehydrogenation

Oxidative dehydrogenation of ethanol (CH_3CH_2OH) to acetaldehyde (CH_3CHO) was used as a probe reaction to evaluate the catalytic activity of the prepared materials, typical conversions are reported in Tables S3 and S4. Under our experimental conditions (WHSV values ranging from 452 to 9052 mol CH_3CH_2OH/mol V-h, reaction temperatures 165–200 °C), the selectivity towards CH_3CHO was in all cases above 99 % with little variance among all samples tested. Regardless of the partial pressure of O_2 used in this study, combustion products such as CO and CO_2 were not detected. The Weisz-Prater criterion (Section I, supporting information) was used to ensure catalytic activity tests were carried under a kinetically controlled regime [60]. To carry out meaningful comparisons of kinetic parameters among the different catalysts, activity tests encompassed a wide range of the CH_3CH_2OH and O_2 partial pressures. The rates obtained were normalized by total vanadium molar loading. This normalization approach assumes all V species in the catalyst participate in the catalytic cycle, a common assumption in the literature evaluating vanadia systems at loadings below or near monolayer coverages [13,34]. Fig. 6 shows the turnover frequency value calculated for the $V/TiO_{0.04}N_{0.98}$ catalyst as a function of CH_3CH_2OH partial pressure (0.5—11 kPa) at three different temperatures (165, 180, and 195 °C), obtained at two different oxygen partial pressures (5 and 0.5 kPa, Fig. 6A and B, respectively). Regardless of O_2 partial pressure and temperature tested, the rates increased linearly with ethanol partial pressure in the low ethanol partial pressure regime ($P_{CH_3CH_2OH} < 2$ kPa) then became independent of this variable at higher ethanol partial pressure, indicating that the surface reaction is controlling reaction rates. At the same time, when comparing rates at two different O_2 partial pressures (Fig. 6A vs. B), we noticed a rate dependence on oxygen partial pressure. Thus, the rates for ethanol ODH are dependent on both ethanol and O_2 partial pressures.

It is well established that oxidative dehydrogenation of short chain alcohols over early transition metal oxides proceeds through a Mars van Krevelen-type redox cycle [33,61]. During the cycle, oxygen exchange between the gas phase and the metal oxide lattice takes place, through sequential reduction and oxidation of the catalytically active species, and the concomitant generation and consumption of oxygen vacancies (O_v). This model can be used to derive a general kinetic expression (Eq. (1)). Scheme 1. provides a graphical representation of the kinetic model; the detailed derivation of Eq.1 is presented in Section II of the supporting information section.

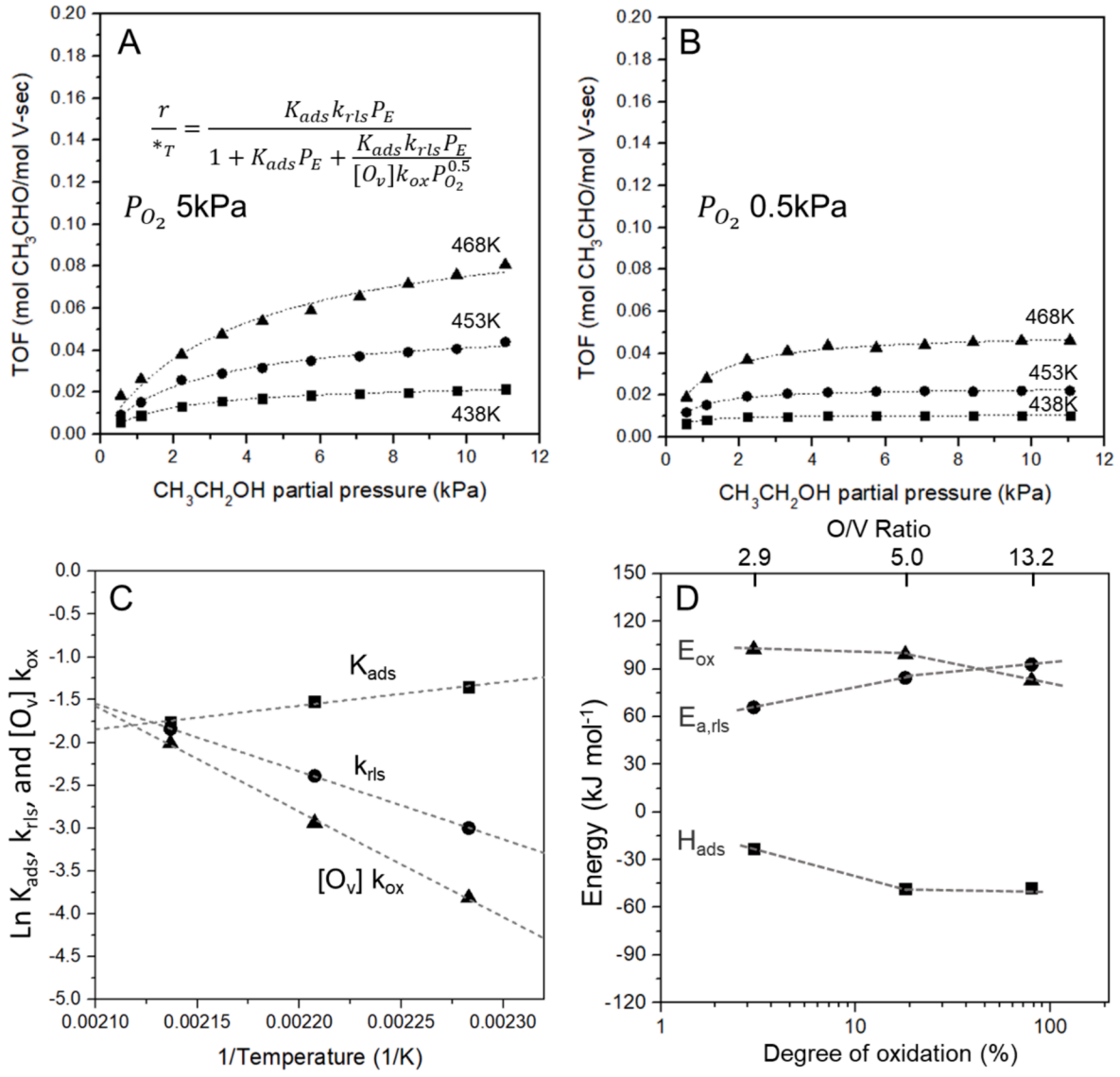

Fig. 6. Dependencies on CH_3CH_2OH partial pressure for the rate of acetaldehyde formation per mol of vanadium on the catalyst (TOF, mol CH_3CHO formation per mol vanadium atom per second) at different temperatures (165 °C, 180 °C, and 195 °C) with (A) 5 kPa O_2 and (B) 0.5 kPa O_2 partial pressure over a $V/TiO_{0.04}N_{0.98}$ catalyst. Dashed lines represent the best fits to Eq. (1). (C) Temperature dependence of the estimated equilibrium constant for the ethanol adsorption step (K_{ads}), the rate constant for the hydrogen abstraction rate-limiting step (k_{rls}), and the rate constant for the vanadia reoxidation step ($[O_v]k_{ox}$) on the basis of the kinetic model represented by Eq(1). (D) Computed heat of adsorption for ethanol on the vanadia active site (H_{ads}), activation energy ($E_{a,rls}$) and energy related to reoxidation steps (E_{ox}) for the $V/TiO_{0.04}N_{0.98}$, $V/TiO_{0.26}N_{0.87}$ and $V/TiO_{1.28}N_{0.36}$ catalyst as a function of the degree of oxidation (bottom horizontal axis) and the molar O/V ratio of the modified TiN_xO_y supports(top horizontal axis). The degree of oxidation was calculated based on the TGA data. H_{ads}, Ea_{rls}, E_{ox} for 0.4 wt%V supported on pristine TiO_2 have been previously reported (−43.0, 66.8, and 47.6 kJ/mol, respectively). [32].

$$\frac{r}{V_T} = \frac{K_{ads}k_{rls}P_{CH_3CH_2OH}}{1 + K_{ads}P_{CH_3CH_2OH} + \frac{K_{ads}k_{rls}P_{CH_3CH_2OH}}{k_{ox}[O_v]P_{O_2}^{0.5}}} \quad (1)$$

*oxi *ads *red

The numerator in Eq. (1) represents the rate limiting step and each term in the denominator corresponds to the surface coverage ratios of specific surface sites (resulting in different vanadia states) in the catalyst present during turnovers: an active oxidized vanadia site (state denoted as *oxi), an oxidized vanadia site bearing an adsorbed ethanol molecule (state denoted as *ads), and reduced vanadia (state denoted as *red). K_{ads} is the equilibrium constant for the reversible ethanol adsorption step (*oxi + CH_3CH_2OH ↔ *ads) and k_{rls} is the rate constant for the rate limiting hydrogen abstraction step. The term k_{ox} represents a lumped rate constant for the catalyst reoxidation steps including the equilibrium constant for molecular oxygen adsorbing on a vacancy (K_{ox}) and the surface concentration of vacancies (O_v) present on the support (titania in this study), which cannot be readily measured. The validity of the kinetic model (Eq.1) was examined by calculating the individual fractional surface coverages representing each state of the vanadium site during turnovers (see details on Supporting Information Section II). The fully oxidized vanadia site is defined as *oxi, the site holding an adsorbed ethanol molecule is defined as *ads, and *red represents the reduced vanadia site after acetaldehyde desorption. The fractional coverages on these three different species are plotted as a function of the CH_3CH_2OH and O_2 partial pressures (Fig. 7). The simulated data clearly suggests that the reduced vanadia species (*red) needs to be incorporated in the rate equation since the coverage of this species is not negligible at high CH_3CH_2OH/O_2 partial pressure ratios.

The estimation of the kinetic parameters usually relies on the assumption of a high oxygen potential on the surface, which makes the fraction of reduced vanadia species negligible, and results in neglecting

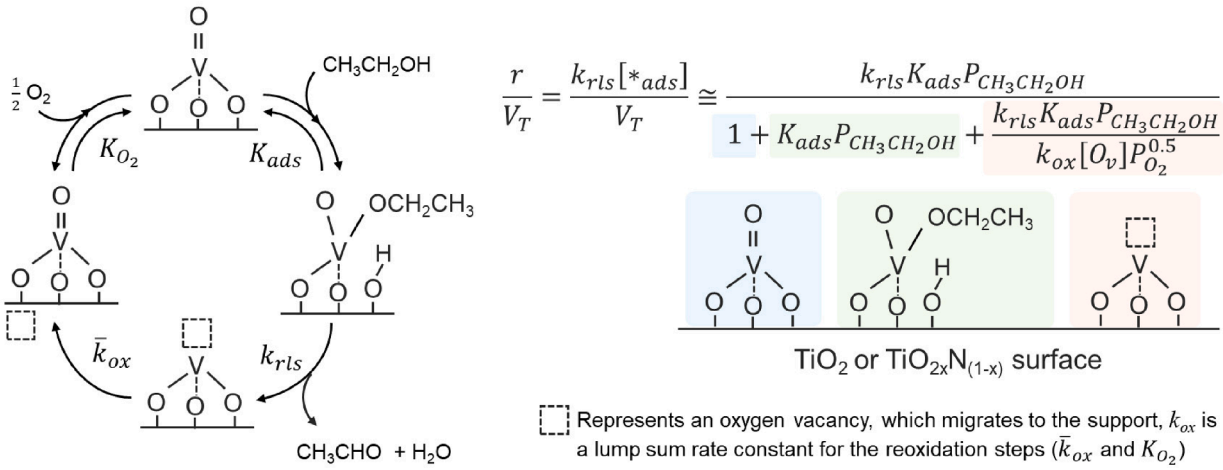

Scheme 1. Graphical representation of the kinetic model used in the derivation of Eq. (1). Details of its derivation are presented in the supporting information section.

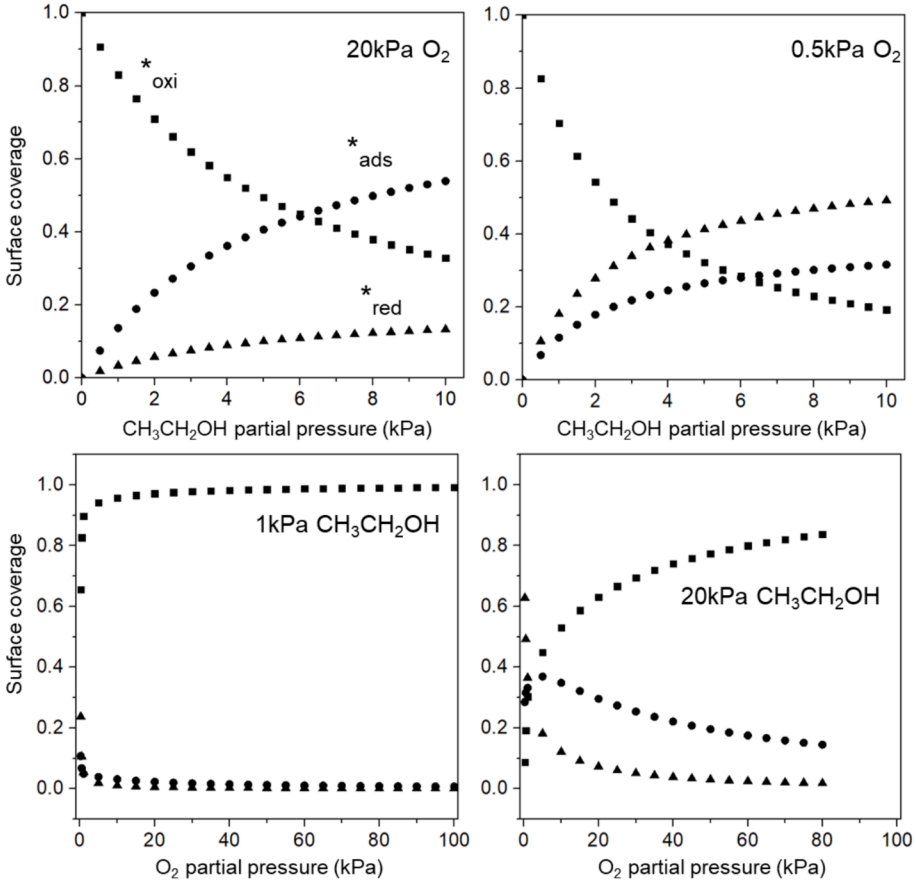

Fig. 7. (Top) Simulated fractional surface coverage of three distinct vanadia states as a function of CH_3CH_2OH partial pressure at 200 °C using two different O_2 constant partial pressures (20 kPa and 0.5 kPa). (Bottom) Simulated surface coverage of three distinct vanadia states as a function of O_2 partial pressure at 200 °C using two different CH_3CH_2OH constant partial pressures (1 kPa and 20 kPa). Symbols, ■, ●, and △ correspond to fractional surface coverage of oxidized (*oxi), ethanol adsorbed (*ads), reduced (*red) vanadia species, being associated to each term in the denominator of Eq.1.

the last term in the denominator in Eq (1). This approach, which offers a relatively simple path for linearization of Eq (1) is valid only at high alcohol/ethanol pressures [31]. The results portrayed in Fig. 7, and discussed above, clearly indicated that this assumption is not valid through all experimental conditions tested in our study. Therefore, we estimated the kinetic parameters by nonlinear regression analysis and the regression curves were fitted to the experimental data shown in Fig. 6A and B (dashed lines). With this aim, nonlinear regression analysis was performed using in-house Matlab programming (iteration method using a multiple nlinfit function with a $< 10^{-4}$ tolerance value). The single rate equation derived to model the dependances on both ethanol and oxygen partial pressures (Eq.1) fits the experimental results well. The estimated three key kinetic parameters (K_{ads}, k_{rls}, and ($[O_v]k_{ox}$) are displayed in an Arrhenius plot in Fig. 5C. We can see that the

equilibrium constant (K_{ads}) decreases while the rate constants for the H-abstraction rate-limiting step (k_{rls}) and vanadia reoxidation step ($[O_v]$ k_{ox}) increases as the temperature rises, indicating the thermodynamic nature of each step-in ethanol ODH over the supported vanadia catalyst: adsorption of ethanol on active vanadia species is exothermic, but both H-abstraction and reoxidation are activated, and possibly endothermic, as proposed in our previous study, when evaluating the energetics of reoxidation of vanadia species anchored on TiO_2 during ethanol partial oxidation [32]. The slopes in the Arrhenius plot yield the heat of ethanol adsorption (H_{ads}), the activation energy ($E_{a,rls}$) and energy associated to reduced vanadia reoxidation (E_{ox}).

We applied this methodology to the kinetic data gathered for the three V/TiO_xN_y catalysts: $V/TiO_{0.04}N_{0.98}$, $V/TiO_{0.26}N_{0.87}$ and $V/TiO_{1.28}N_{0.36}$), and the estimated energy values are plotted as a function of the degree of oxidation (Fig. 6D). As previously stated, the degree of oxidation refers to the oxygen content of the $TiO_{2x}N_{1-x}$ support and is quantitatively linked to the oxygen content of the catalyst. Table S2 provides the information on the V/O ratio in the catalyst calculated for the vanadia catalyst obtained on the different supports. In other words, for the case of the $TiO_{2x}N_{1-x}$ support the degree of oxidation is a descriptor of the oxygen content in the catalyst. Distinct trends are observed in Fig. 6D. First, the heat of ethanol adsorption (H_{ads}) decreases from –23 ($V/TiO_{0.04}N_{0.98}$) to −48 kJ•mol^{-1} ($V/TiO_{0.26}N_{0.87}$) as the degree of oxygen content on the TiO_xN_y support increases. However, further increasing the content of oxygen in the support does not lead to a monotonal decrease, as the heat of ethanol adsorption remains constant at ~48 kJ•mol^{-1} for $V/TiO_{1.28}N_{0.36}$. For the H-abstraction step, its activation energy ($E_{a,rls}$) gradually increases from 66 ($V/TiO_{0.04}N_{0.98}$) to 93 kJ•mol^{-1} ($V/TiO_{1.28}N_{0.36}$). Interestingly, the energy associated to the reoxidation step decreases from 102 ($V/TiO_{0.04}N_{0.98}$) to 83 kJ•mol^{-1} ($V/TiO_{1.28}N_{0.36}$). These values are comparable to the those for V/TiO_2 system with highly dispersed vanadia [33]. We must highlight that the observed differences in the values of the kinetic parameters could originate from the heterogeneous distribution of vanadia cluster sizes which in turn is regulated by the degree of surface oxidation of the support (i.e. oxygen content, section 3.2), and/or the strong interaction between the supported vanadia and the support surface structure. Previous literature [62,63,2] indicates that not all types of surface vanadia species fully participate in redox catalytic turnovers, implying that rooting the variation in the values of the kinetic parameters to a different distribution of vanadia cluster sizes is less likely. By contrast, the comparison of H-abstraction activation energies for ethanol ODH over vanadia catalysts supported on different metal oxides such as titania, zirconia, ceria, silica, and alumina points out to a strong interaction between vanadia and the reducible support [29].

A comparison of the values obtained for the heat of ethanol adsorption (H_{ads}) of vanadia species supported on the oxynitride with the lowest oxygen content (~23 kJ•mol^{-1} for $V/TiO_{0.04}N_{0.98}$) to that with the highest (~48 kJ•mol^{-1} for $V/TiO_{1.28}N_{0.36}$) indicates the presence of a weakly bonded ethoxy species in vanadia anchored on the support with lower oxygen content ($V/TiO_{0.04}N_{0.98}$). Then this adsorbed ethoxy species easily undergoes oxidation, facilitated by low H-abstraction activation energy ($E_{a,rls}$, 66 kJ•mol^{-1}), compared to that obtained on the support with higher oxygen content ($V/TiO_{1.28}N_{0.36}$, $E_{a,rls}$ = 93 kJ•mol^{-1}). However, the resulting reduced vanadia species anchored on $V/TiO_{0.04}N_{0.98}$ *requires a higher energy for the reoxidation step* (E_{ox}, 102 kJ•mol^{-1}) compared to that anchored on the support with higher oxygen content ($V/TiO_{1.28}V_{0.36}$, E_{ox}, 83 kJ•mol^{-1}). This higher energy requirement for the vanadia re-oxidation step, observed for the sample prepared in the support with lowest oxygen content confirms the critical role the support plays in closing the Mars-van Krevelen cycle. [33] Overall, for the ethanol ODH reaction, support lattice oxygen controls the chemical behavior of the vanadia species formed, and thus, its redox kinetics. Though the vanadia reduction steps are regulated by a combination of ethanol adsorption and H abstraction, the vanadia reoxidation process is severely influenced by the availability and/or lability of lattice oxygen, which for the specific case of the TiN_xO_y support is a strong function of the degree of surface oxidation (O/N ratio in the support). This synchronization regulates the overall redox cycle and catalytic activity, which results in a volcano-shaped relationship between the initial turnover frequencies and the presence of lattice oxygen in the support, evaluated either as the degree of oxidation of the TiN_xO_y support, or as the nominal O/V molar ratio in the V/TiN_xO_y catalyst, as clearly depicted in Fig. S8.

3.5. Identification of the catalytically active vanadia moieties: In situ spectroscopic analysis (Raman and NMR)

In situ Raman spectra of two V/TiO_xN_y distinct samples were acquired under reducing and oxidative conditions to elucidate active site structural changes taking place during catalytic turnovers (Fig. 8). To this end, the Raman vanadyl signals of the fully oxidized catalysts under flowing of dry air were measured at 200 °C (Fig. 8a, and d). After this stage, the catalyst was exposed to gaseous ethanol (5 kPa CH_3CH_2OH) for 30 min (data now shown). Previous studies indicate that under these conditions the catalyst undergoes chemical reduction [32]. Following reduction treatment, the sample is exposed to flowing dry air for 30 min. This treatment should reoxidize the vanadia moieties resulting in the recovering of the vanadyl bands. After reoxidation, Raman spectra were measured at 200 °C (Fig. 8b, and e). For the case of the $V/TiO_{0.12}N_{0.94}$ sample, which consists of only dispersed vanadia species, a slight decrease in the vanadyl band intensity and a shift from 1031 cm^{-1} to 1028 cm^{-1} with a shoulder at 1008 cm^{-1} is observed after the reoxidation step (Fig. 8b). A longer time of exposure to dry air at 200 °C did not result in a recovery of the band to its initial position (data not shown). The Raman band shifts back to its original position (1031 cm^{-1}) only if reoxidation takes place at 400 °C (Fig. 8c). In contrast, for the case of the $V/TiO_{1.28}N_{0.36}$ catalyst, where both dispersed vanadia and V_2O_5 nano-crystallites are present, the Raman band at 992 cm^{-1}, corresponding to the vanadyl stretching of V_2O_5 nano-crystallites and that at 1031 cm^{-1} associated with highly dispersed vanadia species completely disappeared upon exposure to gas phase ethanol. After sequential treatment with air at 200 °C, the band at 992 cm^{-1} cannot be recovered (Fig. 8e), contrasting to the behavior of the band at 1031 cm^{-1} which recovered (although with a slight shift, likely arising from some restructuring of vanadia moieties). Only a more aggressive oxidation treatment (dry air at 400 °C) results in the full recovery of the band at 992 cm^{-1} (Fig. 8f). This dynamic behavior during reduction-reoxidation cycles for two catalysts with different distribution of vanadia indicate that the vanadia species responsible for the broad Raman band peaking at 1031 cm^{-1} with a shoulder at 1008 cm^{-1} are the active redox species participating in turnovers for the case of ethanol ODH at low temperatures (~200 °C).

The chemical environment of oxide materials can have a dramatic effect on the structures and properties of the catalytic materials. Reactions at higher temperatures where water readily desorbs results in VOx structures that are analogous to those after dehydrating conditions when not directly interacting with reactants [64,65]. At lower temperatures in the presence of moisture, hydrolysis of the V-O-Support bonds can take place alongside agglomeration of isolated VOx structures [66,58]. The reactions reported herein are conducted at a modest ~473 K and produce water, resulting in the likely presence of changing Vox structures during the reaction. To assess any potential significant changes in Vox speciation, we have conducted in situ NMR measurements on materials which have been exposed to the chemical reactor environment.

^{51}V MAS NMR spectra of samples exposed to this sequential reducing and oxidating treatment ("Reoxidized") are shown on the right side of Fig. 5. As discussed in Section 3.2, after initial dehydration at 300 °C in air, a range of vanadia species is observed. For the case of the $V/TiO_{0.04}N_{0.98}$ sample, the main features (515–530 ppm and ~560 ppm) were consistent with highly dispersed vanadia monomers and dimers are

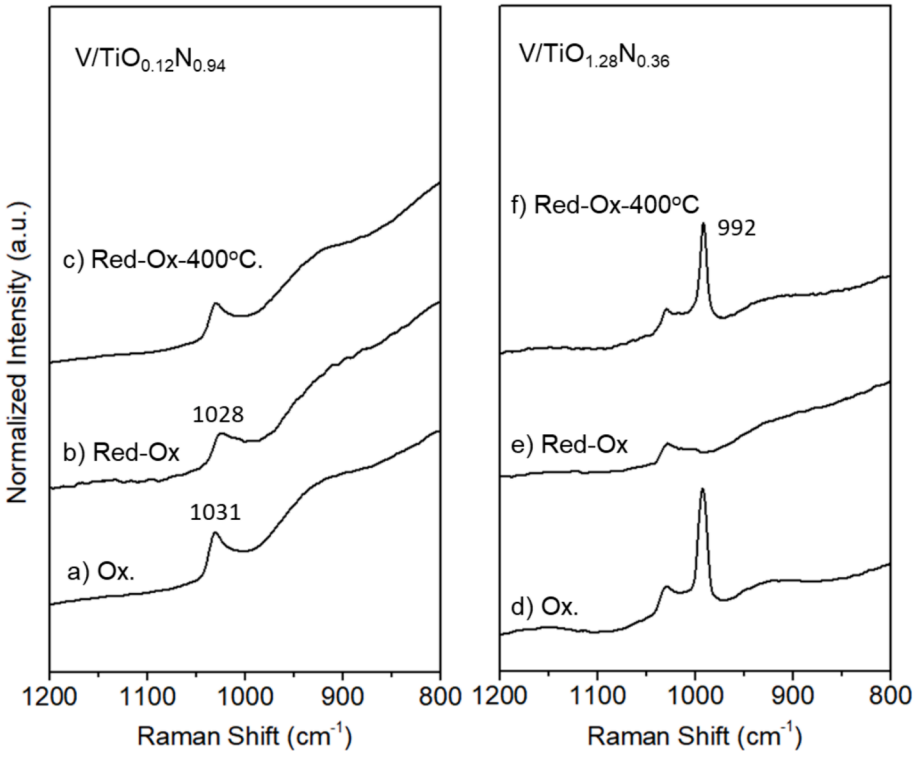

Fig. 8. In situ Raman spectra of V = O stretching of $V/TiO_{0.12}N_{0.94}$ (a, b, and c) and $V/TiO_{1.28}N_{0.36}$ (d, e, and f). Spectra a, and d were measured at 200 °C under dry air gas flow. Spectra b, and e were obtained after a sequential treatment: 5 kPa CH_3CH_2OH at 200 °C for 30 min followed by dry air (50 ml•min^{-1}) at 200 °C for 30 min. Spectra c, and f were measured after sequentially exposing the same samples to a more aggressive re-oxidation treatment (dry air, 50 ml•min^{-1} at 400 °C, 40 mins).

easily identifiable. In contrast the $V/TiO_{0.26}N_{0.87}$ sample presented features consistent with large oligomeric vanadia domains. Subsequent reduction in an C_2H_5OH/N_2 environment for one hour at 200 °C resulted in the elimination of nearly all ^{51}V NMR signals due to the reduction of V^{+5} centers to paramagnetic species which cannot be readily observed with NMR spectroscopy and impair the observation of nearby nuclear spins (Figure S9, "Reduced" spectra). After reoxidation in air at the reaction temperature (200 °C), many of the vanadia signals are restored, but there is a detectable redistribution of species favoring reformation of monomeric and dimeric vanadia (downfield of −600 ppm), suggesting either an increment of the amount of highly dispersed vanadia species or an incomplete reoxidation of the larger vanadia domains. The spectral changes taking place after reducing/re-oxidizing treatment are even more dramatic for the case of the support $V/TiO_{0.26}N_{0.87}$ sample. Again, the relative intensity of the primarily bulk-like feature at −614 ppm decreases in favor of well dispersed dimeric and oligomeric species (peaks between −560 and −700 ppm), which again could be the result of either a redistribution of species during treatment (implying large nanocrystalline vanadia domains are dispersed under the sequential reduction/oxidation treatment) or the incapacity of the large nanocrystalline vanadia cluster to reoxidize, under reaction conditions, from a reduced state back to V^{+5}. As discussed in the sections above, the kinetic analysis of the energetics of the reoxidation step and the in situ Raman data clearly indicates that it is the lack of ability of the large vanadium species to re-oxidize under these conditions which is responsible for the spectral changes observed in the NMR. It is possible however that during catalysis, the supported vanadia species could be mobile over the surface of the metal oxide support and aggregate. This phenomenon, however, is regulated by a variety of factors, among them: vanadia loading, the thermal history of the sample, the vanadia/support interaction, the reaction temperature during catalysis, and the distinct surface oxidation/reduction potentials set by the gas phase. In our case, the metal support interaction between vanadia and TiO_2 moieties is relatively strong (as opposed to, for instance, SiO_2), and the mild reaction conditions used in this study (165–200 °C), contrasts the conditions used for alkane ODH (400 °C–550 °C), where vanadia moieties experience severe re-speciation under reaction conditions [67]. In this context, the spectroscopic data obtained (Figs. 5 and 8), indicate that although vandia re-speciation could take place, monomeric and dimeric vanadia species remain in the catalyst surface on the samples with high nitrogen content ($V/TiO_{0.04}N_{0.98}$ $V/TiO_{0.12}N_{0.94}$) after treatment in ethanol at 200 °C.

3.6. *The key role of the titania oxygen lattice in the vanadia reoxidation step*

From the examination in section 3.3, what is particularly interesting is that the energy values associated to the reoxidation steps (E_{ox}) differ from those reported earlier for VO_x/TiO_2 systems (47.6 kJ•mol^{-1} [33] vs. ~90 kJ•mol^{-1} in this study). We could attribute this change to the different distribution of vanadia species and their local environment in respect to lattice oxygen from the support, since in the aforementioned study, only 0.4 wt% of vanadia was incorporated on titania. Hence in that specific system there are more titania sites able to generate lattice oxygen vacancies, which are responsible for the adsorption of gaseous oxygen and likely regulate the vanadium reoxidation step [33]. On the contrary, for the case of catalysts used in this study, the quantity of accessible lattice oxygen is much lower since the support is largely comprised of nitrogen and, furthermore vanadia is present at near or above nominal monolayer coverages, hence hindering the accessibility of gaseous oxygen to any potential oxygen vacancies present on the Ti-O sites of the support. To gain a deeper insight on these phenomena, we further examined the energetics of catalyst reduction and reoxidation by restricting the support's ability to form active oxygen sites. In these sets of experiments, we used a series of conventional V/TiO_2 catalysts, prepared using conventional TiO_2, with different vanadia loadings (0.4, 0.8,

1.2, and 3.6 wt%). The distribution of vanadia species for this set of samples was assessed using in situ Raman spectroscopy.

(Fig.S5). Based on the Raman data, highly dispersed vanadia was observed up to V loadings of 1.2 wt% while above this value polymeric and V_2O_5 nano-crystallites form. As vanadia coverage increases up to 1.2 wt% (Fig. 9) increasing energy requirements are observed in both steps required for vanadia reduction stage (H_{ads}+$E_{a,rls}$) and also for that of the vanadia reoxidation step (E_{ox}). These two values remain constant at V coverages higher than 1.2 wt%. These observations, combined with those depicted in Section 3.1, showing that terminal hydroxyl groups in the support are responsible for the formation of the dispersed vanadia moieties, lead us to hypothesize that *the catalytic activity of even well dispersed vanadia is regulated by the concentration of the local lattice O present in the support*. At the lowest V coverage (0.4 wt%), the dispersed vanadia are localized in a higher "re-oxidizing" local environment, i.e. more accessible adjacent lattice oxygen. As vanadia loading increases up to near saturation coverages (~1.2 wt%), vanadia domains get sterically closer to each other by consuming terminal hydroxyls groups originally present in the TiO_2 support (which serve as anchoring points for vanadia). This process concomitantly leads to the loss in accessibility to support lattice oxygens, affecting overall activity. Our results indicate that there is a dramatic consequence in thermal parameters (apparent activation energy, energy requirement for reoxidation step) of the active vanadia species depending not only on the vanadia coverage but also on the environment where the active vanadia species sits. In other words, the differences between the values of the thermal parameters obtained for vanadium supported on the TiO_xN_y (Fig. 6D), and those obtained on vanadia supported on pristine TiO_2 (Fig. 9) are a consequence not only of the vanadia state of dispersion (monomer vs oligomer) but also of the local environment surrounding the active vanadia moieties, specifically of the proximity of "active" oxygen centers, able to reoxidize the vanadia cluster during catalytic turnovers. This phenomenon arises in the case of identical vanadia coverages on surfaces with different "active" oxygen support lattice content (Fig. 6D) or when vanadia coverages increases at the expense of the "active" oxygen support lattice content (Fig. 9). Whether the reoxidation capacity of this "active" oxygen is regulated by oxygen mobility or lability remains unknown, however it is clearly tied to the redox ability of the support. Maximizing catalytic performance of individual active supported vanadia species is thus possible if vanadia moieties are dispersed and localized far from each other in a higher "re-oxidizing" local environment.

4. Conclusion

Our results strongly indicate that the formation of catalytically active monomeric and dimeric vanadia species over titania takes place at the expense of the terminal hydroxyls groups on the support, while the consumption of titania bridged hydroxyls is linked to the formation of polymeric vanadia and V_2O_5 nano crystallites. A detailed inspection into the support surface morphology and evaluation of catalytic activity indicates that the intrinsic kinetic parameters of the kinetically relevant steps for ethanol oxidative dehydrogenation (heat of adsorption, hydrogen abstraction activation energy, and the energetics of reoxidation steps) depend not only of the vanadia cluster size, but also of the local environment surrounding the vanadia species and vanadia coverage, where the ability of the support to provide oxygen during the vanadia reoxidation step of the Mars-van Krevelen cycle plays a critical role for catalytic activity.

CRediT authorship contribution statement

Dongmin Yun: Writing – original draft, Visualization, Validation, Methodology, Investigation, Formal analysis, Data curation, Conceptualization. **Nicolas R. Jaegers:** Writing – original draft, Validation, Formal analysis, Data curation. **Jian Zhi Hu:** Writing – review & editing, Supervision. **Adrian M. Hucal:** Data curation. **José E. Herrera:** Writing – review & editing, Supervision. **Yong Wang:** Writing – review & editing, Supervision.

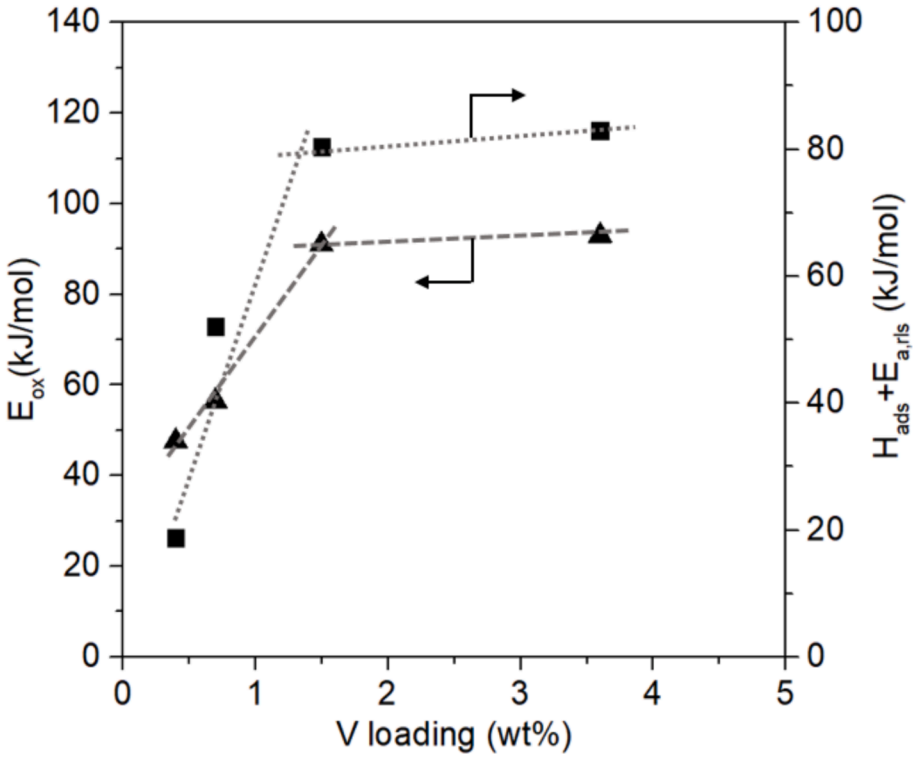

Fig. 9. Energy associated to the reoxidation step (triangles), and the sum of heat of adsorption and H-abstraction energy (squares) as a function of V loading over supported vanadia on pristine TiO_2 catalysts.

Declaration of competing interest

The authors declare that they have no known competing financial interests or personal relationships that could have appeared to influence the work reported in this paper.

Data availability

No data was used for the research described in the article.

Acknowledgements

This research was supported by the U.S Department of Energy, Office of Basic Energy Sciences, Division of Chemical Sciences, Biosciences, and Geosciences (DE-AC05-RL01830, FW-47319). The financial support from the Natural Sciences and Engineering Research Council of Canada, and Suncor energy Inc. is gratefully acknowledged. NMR experiments were conducted in the Environmental Molecular Sciences Laboratory (EMSL), a national scientific user facility sponsored by the Department of Energy's Office of Biological and Environmental Research at Pacific Northwest National Laboratory (PNNL), using a Bruker 600MHz NMR spectrometer acquired with support from the US Department of Energy, Office of Science, Office of Basic Energy Sciences (Project Number 66628). Electron Microscopy imaging was carried out at the Canadian Centre for Electron Microscopy (CCEM) located in McMaster University, Canada..The support from the staff at both EMSL and CCEM is acknowledged.

Appendix A. Supplementary material

Supplementary material to this article can be found online at https://doi.org/10.1016/j.jcat.2024.115642.

References

[1] C.D. Baertsch, K.T. Komala, Y.-H. Chua, E. Iglesia, Genesis of brønsted acid sites during dehydration of 2-butanol on tungsten oxide catalysts, J. Catal. 205 (2002) 44–57, https://doi.org/10.1006/jcat.2001.3426.

[2] D. Yun, J.E. Herrera, A novel methodology for in situ redox active site titration of TiO_2-supported vanadia during ethanol partial oxidation catalysis, J. Catal. 350 (2017) 72–85, https://doi.org/10.1016/j.jcat.2017.04.001.

[3] M. Cargnello, V.V.T. Doan-Nguyen, T.R. Gordon, R.E. Diaz, E. a Stach, R.J. Gorte, P. Fornasiero, C.B. Murray, Control of metal nanocrystal size reveals metal-support interface role for ceria catalysts, Science 341 (2013) 771–773, https://doi.org/10.1126/science.1240148.

[4] M.O. Guerrero-Pérez, J.M. Rosas, R. López-Medina, M.A. Bañares, J. Rodríguez-Mirasol, T. Cordero, On the nature of surface vanadium oxide species on carbons, J. Phys. Chem. C 116 (2012) 20396–20403, https://doi.org/10.1021/jp305853b.

[5] R. Chlosta, G. Tzolova-Müller, R. Schlögl, C. Hess, Nature of dispersed vanadium oxide: influence of the silica support structure and synthesis methods, Catal. Sci. Technol. 1 (2011) 1175, https://doi.org/10.1039/c1cy00062d.

[6] J.A. Rodriguez, D. Stacchiola, Catalysis and the nature of mixed-metal oxides at the nanometer level: special properties of MOx/TiO2(110) M= V, W, Ce surfaces, Phys. Chem. Chem. Phys. 12 (2010) 9557–9565, https://doi.org/10.1039/C003665J.

[7] M. Baron, H. Abbott, O. Bondarchuk, D. Stacchiola, A. Uhl, S. Shaikhutdinov, H.-J. Freund, C. Popa, M.V. Ganduglia-Pirovano, J. Sauer, Resolving the atomic structure of vanadia monolayer catalysts: monomers, trimers, and oligomers on ceria, Angew. Chem. Int. Ed. Engl. 48 (2009) 8006–8009, https://doi.org/10.1002/anie.200903085.

[8] Z. Wu, A.J. Rondinone, I.N. Ivanov, S.H. Overbury, Structure of vanadium oxide supported on ceria by multiwavelength Raman spectroscopy, J. Phys. Chem. c. 115 (2011) 25368–25378, https://doi.org/10.1021/jp2084605.

[9] D. Nitsche, C. Hess, Structure of isolated vanadia and titania: a deep UV Raman, UV-Vis, and IR spectroscopic study, J. Phys. Chem. C 120 (2016) 1025–1037, https://doi.org/10.1021/acs.jpcc.5b10317.

[10] H.H. Kristoffersen, H.L. Neilson, S.K. Buratto, H. Metiu, Stability of V_2O_5 supported on titania in the presence of water, bulk oxygen vacancies, and adsorbed oxygen atoms, J. Phys. Chem. C 121 (2017) 8444–8451, https://doi.org/10.1021/acs.jpcc.7b00745.

[11] J.S. Elias, N. Artrith, M. Bugnet, L. Giordano, G.A. Botton, A.M. Kolpak, Y. Shao-Horn, Elucidating the nature of the active phase in copper/ceria catalysts for CO oxidation, ACS Catal. 6 (2016) 1675–1679, https://doi.org/10.1021/acscatal.5b02666.

[12] L. Nie, D. Mei, H. Xiong, B. Peng, Z. Ren, X.I.P. Hernandez, A. DeLaRiva, M. Wang, M.H. Engelhard, L. Kovarik, A.K. Datye, Y. Wang, Activation of surface lattice oxygen in single-atom Pt/CeO_2 for low-temperature CO oxidation, Science 80 (358) (2017) 1419–1423, https://doi.org/10.1126/science.aao2109.

[13] A. Zabilska, M. Zabilskiy, R.J.G. Nuguid, A.H. Clark, I.I. Sadykov, M. Nachtegaal, O. Kröcher, O.V. Safonova, Activity trend origin of ethanol oxidative dehydrogenation over VOx/CeO_2, Angew. Chemie Int. Ed. (2023) 202301297, https://doi.org/10.1002/anie.202301297.

[14] W.T. Broomhead, W. Tian, J.E. Herrera, Y.-H.-C. Chin, Kinetic coupling of redox and acid chemistry in methanol partial oxidation on vanadium oxide catalysts, ACS Catal. 12 (2022) 11801–11820, https://doi.org/10.1021/acscatal.2c01852.

[15] L. Barrio, M. Estrella, G. Zhou, W. Wen, J.C. Hanson, A.B. Hungría, A. Hornés, M. Fernández-García, A. Martínez-Arias, J.A. Rodriguez, Unraveling the active site in copper−ceria systems for the water−gas shift reaction: in situ characterization of an inverse powder CeO_2−x/CuO−Cu Catalyst, J. Phys. Chem. C 114 (2010) 3580–3587, https://doi.org/10.1021/jp910342b.

[16] A. Dinse, B. Frank, C. Hess, D. Habel, R. Schomäcker, Oxidative dehydrogenation of propane over low-loaded vanadia catalysts: impact of the support material on kinetics and selectivity, J. Mol. Catal. A Chem. 289 (2008) 28–37, https://doi.org/10.1016/j.molcata.2008.04.007.

[17] C.A. Carrero, R. Schlögl, I.E. Wachs, R. Schomaecker, Critical literature review of the kinetics for the oxidative dehydrogenation of propane over well-defined supported vanadium oxide catalysts, ACS Catal. 4 (2014) 3357–3380, https://doi.org/10.1021/cs5003417.

[18] L. Schumacher, J. Weyel, C. Hess, Unraveling the active vanadium sites and adsorbate dynamics in VOx/CeO_2 oxidation catalysts using transient IR spectroscopy, J. Am. Chem. Soc. 144 (2022) 14874–14887, https://doi.org/10.1021/jacs.2c06303.

[19] P. Kube, B. Frank, R. Schlögl, A. Trunschke, Isotope studies in oxidation of propane over vanadium oxide, ChemCatChem. 9 (2017) 3434, https://doi.org/10.1002/cctc.201701443.

[20] L. Schumacher, J. Pfeiffer, J. Shen, T. Gutmann, H. Breitzke, G. Buntkowsky, K. Hofmann, C. Hess, Collaborative mechanistic effects between vanadia and titania during the oxidative dehydrogenation of propane investigated by operando and transient spectroscopies, ACS Catal. 13 (2023) 8139–8160, https://doi.org/10.1021/acscatal.3c01404.

[21] Q. Shi, Y. Li, Y. Zhou, S. Miao, N. Ta, E. Zhan, J. Liu, W. Shen, The shape effect of TiO_2 in VOx/TiO_2 catalysts for selective reduction of NO by NH_3, J. Mater. Chem. A 3 (2015) 14409–14415, https://doi.org/10.1039/c5ta02897c.

[22] J.A. Dumesic, N.-Y. Topsøe, H. Topsøe, Y. Chen, T. Slabiak, Kinetics of Selective catalytic reduction of nitric oxide by ammonia over vanadia/titania, J. Catal. 163 (1996) 409–417, https://doi.org/10.1006/jcat.1996.0342.

[23] I.E. Wachs G. Deo B.M. Weckhuysen A. Andreini M.A. Vuurman M. De Boer M.D. Amiridis Selective Catalytic Reduction of NO with NH3 over Supported Vanadia Catalysts, 221 (1996) 211–221.

[24] P. Ji, X. Gao, X. Du, C. Zheng, Z. Luo, K. Cen, Relationship between the molecular structure of V_2O_5/TiO_2 catalysts and the reactivity of SO_2 oxidation, Catal. Sci. Technol. 6 (2016) 1187–1194, https://doi.org/10.1039/C5CY00867K.

[25] B. Schimmoeller, H. Schulz, A. Ritter, A. Reitzmann, B. Kraushaar-Czarnetzki, A. Baiker, S.E. Pratsinis, Structure of flame-made vanadia/titania and catalytic behavior in the partial oxidation of o-xylene, J. Catal. 256 (2008) 74–83, https://doi.org/10.1016/j.jcat.2008.03.005.

[26] Y. Li, Z. Wei, F. Gao, L. Kovarik, C.H.F. Peden, Y. Wang, Effects of CeO_2 support facets on VOx/CeO_2 catalysts in oxidative dehydrogenation of methanol, J. Catal. 315 (2014) 15–24, https://doi.org/10.1016/j.jcat.2014.04.013.

[27] T.V. Andrushkevich, V.V. Kaichev, Y.A. Chesalov, A.A. Saraev, V.I. Buktiyarov, Selective oxidation of ethanol over vanadia-based catalysts: The influence of support material and reaction mechanism, Catal. Today. 279 (2017) 95–106, https://doi.org/10.1016/j.cattod.2016.04.042.

[28] S.P. Price, X. Tong, C. Ridge, H.L. Neilson, J.W. Buffon, J. Robins, H. Metiu, M. T. Bowers, S.K. Buratto, Catalytic oxidation of methanol to formaldehyde by mass-selected vanadium oxide clusters supported on a TiO_2(110) surface, J. Phys. Chem. A 118 (2014) 8309–8313, https://doi.org/10.1021/jp5011378.

[29] B. Beck, M. Harth, N.G. Hamilton, C. Carrero, J.J. Uhlrich, A. Trunschke, S. Shaikhutdinov, H. Schubert, H.-J. Freund, R. Schlögl, J. Sauer, R. Schomäcker, Partial oxidation of ethanol on vanadia catalysts on supporting oxides with different redox properties compared to propane, J. Catal. 296 (2012) 120–131, https://doi.org/10.1016/j.jcat.2012.09.008.

[30] A. Iglesias-Juez, M.V. Martínez-Huerta, E. Rojas-García, J.-M. Jehng, M.A. Bañares, On the nature of the unusual redox cycle at the vanadia ceria interface, J. Phys. Chem. C 122 (2018) 1197–1205, https://doi.org/10.1021/acs.jpcc.7b09832.

[31] M. Ek, Q.M. Ramasse, L. Arnarson, P. Georg Moses, S. Helveg, Visualizing atomic-scale redox dynamics in vanadium oxide-based catalysts, Nat. Commun. 8 (2017), https://doi.org/10.1038/s41467-017-00385-y.

[32] D. Yun, Y. Song, J.E. Herrera, Supported vanadium oxide clusters in partial oxidation processes: catalytic consequences of size and electronic structure, ChemCatChem. 9 (2017) 3655–3669, https://doi.org/10.1002/cctc.201700503.

[33] D. Yun, Y. Wang, J.E. Herrera, Ethanol partial oxidation over VOx /TiO_2 catalysts: the role of titania surface oxygen on vanadia reoxidation in the mars–van krevelen mechanism, ACS Catal. 8 (2018) 4681–4693, https://doi.org/10.1021/acscatal.7b03327.

[34] D. Yun, Y. Song, J.E. Herrera, Electronic structure changes introduced by nitrogen on the N-doped VOx/TiO_2 system: consequences on partial oxidation catalysis, Mol. Catal. 448 (2018) 122–134, https://doi.org/10.1016/j.mcat.2018.02.001.

[35] A. Zabilska, A.H. Clark, B.M. Moskowitz, I.E. Wachs, Y. Kakiuchi, C. Copéret, M. Nachtegaal, O. Kröcher, O.V. Safonova, Redox dynamics of active VOx sites promoted by TiOx during oxidative dehydrogenation of ethanol detected by

operando quick XAS, JACS Au. 2 (2022) 762–776, https://doi.org/10.1021/jacsau.2c00027.
[36] Z. Zhang, X. Wang, J. Long, Q. Gu, Z. Ding, X. Fu, Nitrogen-doped titanium dioxide visible light photocatalyst : spectroscopic identification of photoactive centers, J. Catal. 276 (2010) 201–214, https://doi.org/10.1016/j.jcat.2010.07.033.
[37] R. Asahi, T. Morikawa, H. Irie, T. Ohwaki, Nitrogen-doped titanium dioxide as visible-light-sensitive photocatalyst : designs, Develop. Prospects (2014), https://doi.org/10.1021/cr5000738.
[38] E.A. Davis, N.F. Mott, Conduction in non-crystalline systems V. conductivity, optical absorption and photoconductivity in amorphous semiconductors, Philos. Mag. 22 (1970) 903–922, https://doi.org/10.1080/14786437008221061.
[39] N.C. Saha, H.G. Tompkins, Titanium nitride oxidation chemistry: An x-ray photoelectron spectroscopy study, J. Appl. Phys. 72 (1992) 3072–3079, https://doi.org/10.1063/1.351465.
[40] N.R. Mucha, J. Som, S. Shaji, S. Fialkova, P.R. Apte, B. Balasubramanian, J. E. Shield, M. Anderson, D. Kumar, Electrical and optical properties of titanium oxynitride thin films, J. Mater. Sci. 55 (2020) 5123–5134, https://doi.org/10.1007/s10853-019-04278-x.
[41] J.Z. Zhang, Metal oxide nanomaterials for solar hydrogen generation from photoelectrochemical water splitting, MRS Bull. 36 (2011) 48–55, https://doi.org/10.1557/mrs.2010.9.
[42] Y. Bao, C. Li, K. Domen, F. Zhang, Strategies and methods of modulating nitrogen-incorporated oxide photocatalysts for promoted water splitting, Accounts Mater. Res. 3 (2022) 449–460, https://doi.org/10.1021/accountsmr.1c00271.
[43] H.-Y. Chen, F.-H. Lu, Oxidation behavior of titanium nitride films, J. Vac. Sci. Technol. A Vacuum, Surfaces, Film. 23 (2005) 1006–1009, https://doi.org/10.1116/1.1914815.
[44] J. Desmaison, P. Lefort, M. Billy, Oxidation mechanism of titanium nitride in oxygen, Oxid. Met. 13 (1979) 505–517, https://doi.org/10.1007/BF00812775.
[45] H.G. Tompkins, Oxidation of titanium nitride in room air and in dry O_2, J. Appl. Phys. 70 (1991) 3876–3880, https://doi.org/10.1063/1.349194.
[46] A. Murano, H. Funabiki, T. Sekiya, Change in electronic state of nitrogen in oxidized titanium nitride, J. Phys. Chem. Solids. 168 (2022) 110817, https://doi.org/10.1016/j.jpcs.2022.110817.
[47] M. Schraml-Marth, A. Wokaun, A. Baiker, Grafting of V_2O_5 monolayers onto TiO_2 from alkoxide precursors: a diffuse reflectance FTIR study, J. Catal. 124 (1990) 86–96, https://doi.org/10.1016/0021-9517(90)90105-S.
[48] A. Vittadini, A. Selloni, Periodic density functional theory studies of vanadia−titania catalysts: structure and stability of the oxidized monolayer, J. Phys. Chem. B 108 (2004) 7337–7343, https://doi.org/10.1021/jp037869z.
[49] H. Lin, J. Long, Q. Gu, W. Zhang, R. Ruan, Z. Li, X. Wang, In situ IR study of surface hydroxyl species of dehydrated TiO_2: towards understanding pivotal surface processes of TiO_2 photocatalytic oxidation of toluene, Phys. Chem. Chem. Phys. 14 (2012) 9468–9474, https://doi.org/10.1039/C2CP40893G.
[50] C. Deiana, E. Fois, S. Coluccia, G. Martra, Surface structure of TiO_2 P25 nanoparticles: Infrared study of hydroxy groups on coordinative defect sites, J. Phys. Chem. C 114 (2010) 21531–21538, https://doi.org/10.1021/jp107671k.
[51] H.-J. Freund, Model studies in heterogeneous catalysis, Chem. Eur. J. 16 (2010) 9384–9397, https://doi.org/10.1002/chem.201001724.
[52] L. Burcham, G. Deo, X. Gao, I. Wachs, In situ IR, Raman, and UV-Vis DRS spectroscopy of supported vanadium oxide catalysts during methanol oxidation, Top. Catal. 11–12 (2000) 85–100, https://doi.org/10.1023/A:1027275225668.
[53] C.A. Carrero, C.J. Keturakis, A. Orrego, R. Schomacker, I.E. Wachs, Anomalous reactivity of supported V_2O_5 nanoparticles for propane oxidative dehydrogenation: influence of the vanadium oxide precursor, Dalt. Trans. 42 (2013) 12644–12653, https://doi.org/10.1039/C3DT50611H.
[54] G.T. Went, L. Leu, A.T. Bell, Quantitative structural analysis of dispersed vanadia species in TiO_2(anatase)-supported V_2O_5, J. Catal. 134 (1992) 479–491, https://doi.org/10.1016/0021-9517(92)90336-G.
[55] T. Kentri, A. Tsevis, S. Boghosian, Heterogeneity of the vanadia phase dispersed on titania. Co-existence of distinct mono-oxo VOx sites, Dalt, Trans. 52 (2023) 7495–7511, https://doi.org/10.1039/d3dt00749a.
[56] Z. Feng, J. Lu, H. Feng, P.C. Stair, J.W. Elam, M.J. Bedzyk, Catalysts transform while molecules react: an atomic-scale view, J. Phys. Chem. Lett. 4 (2012) 285–291, https://doi.org/10.1021/jz301859k.
[57] J.Z. Hu, S. Xu, W.-Z. Li, M.Y. Hu, X. Deng, D.A. Dixon, M. Vasiliu, R. Craciun, Y. Wang, X. Bao, C.H.F. Peden, Investigation of the structure and active sites of TiO_2 nanorod supported VOx catalysts by high-field and fast-spinning 51 V MAS NMR, ACS Catal. 5 (2015) 3945–3952, https://doi.org/10.1021/acscatal.5b00286.
[58] N.R. Jaegers, C. Wan, M.Y. Hu, M. Vasiliu, D.A. Dixon, E. Walter, I.E. Wachs, Y. Wang, J.Z. Hu, Investigation of silica-supported vanadium oxide catalysts by high-field 51V magic-angle spinning NMR, J. Phys. Chem. C (2017), https://doi.org/10.1021/acs.jpcc.7b01658.
[59] N.R. Jaegers, J.K. Lai, Y. He, E. Walter, D.A. Dixon, M. Vasiliu, Y. Chen, C. Wang, M.Y. Hu, K.T. Mueller, I.E. Wachs, Y. Wang, J.Z. Hu, Mechanism by which tungsten oxide promotes the activity of supported V_2O_5/TiO_2 catalysts for NOX abatement: structural effects revealed by 51V MAS NMR spectroscopy, Angew. Chemie - Int. Ed. 58 (2019) 12609–12616, https://doi.org/10.1002/anie.201904503.
[60] S. Ted Oyama, G.-N. Yun, S.-J. Ahn, K.K. Bando, A. Takagaki, R. Kikuchi, How to scrutinize adsorbed intermediates observed by in situ spectroscopy: Analysis of Coverage Transients (ACT), J. Catal. 394 (2021) 273–283, https://doi.org/10.1016/j.jcat.2020.10.029.
[61] A.R. Puigdollers, P. Schlexer, S. Tosoni, G. Pacchioni, Increasing oxide reducibility: the role of metal/oxide interfaces in the formation of oxygen vacancies, ACS Catal. 7 (2017) 6493–6513, https://doi.org/10.1021/acscatal.7b01913.
[62] M.D. Argyle, K. Chen, C. Resini, C. Krebs, A.T. Bell, E. Iglesia, In situ UV-visible assessment of extent of reduction during oxidation reactions on oxide catalysts, Chem. Commun. 16 (2003) 2082–2083, https://doi.org/10.1039/b305264h.
[63] M.D. Argyle, K. Chen, C. Resini, C. Krebs, A.T. Bell, E. Iglesia, Extent of reduction of vanadium oxides during catalytic oxidation of alkanes measured by in-situ UV−Visible spectroscopy, J. Phys. Chem. B 108 (2004) 2345–2353, https://doi.org/10.1021/jp030989m.
[64] J.-K. Lai, N.R. Jaegers, B.M. Lis, M. Guo, M.E. Ford, E. Walter, Y. Wang, J.Z. Hu, I. E. Wachs, Structure–activity relationships of hydrothermally aged titania-supported vanadium–tungsten oxide catalysts for SCR of NO_x Emissions with NH_3, ACS Catal. 11 (2021) 12096–12111, https://doi.org/10.1021/acscatal.1c02130.
[65] N.R. Jaegers, J.-K. Lai, Y. He, E. Walter, D.A. Dixon, M. Vasiliu, Y. Chen, C. Wang, M.Y. Hu, K.T. Mueller, I.E. Wachs, Y. Wang, J.Z. Hu, Mechanism by which tungsten oxide promotes the activity of supported V_2O_5/TiO_2 catalysts for NO_X abatement: structural effects revealed by 51V MAS NMR spectroscopy, Angew Chemie. 131 (2019) 12847, https://doi.org/10.1002/ange.201908846.
[66] N.R. Jaegers, Y. Wang, J.Z. Hu, I.E. Wachs, Impact of hydration on supported V_2O_5/TiO_2 catalysts as explored by magnetic resonance spectroscopy, J. Phys. Chem. C 125 (2021) 16766–16775, https://doi.org/10.1021/acs.jpcc.1c04150.
[67] P. Djinović, J. Zavašnik, J. Teržan, I. Jerman, Role of CO_2 during oxidative dehydrogenation of propane over bulk and activated-carbon supported cerium and vanadium based catalysts, Catal. Lett. 151 (2021) 2816–2832, https://doi.org/10.1007/s10562-020-03519-y.